POLITECNICO DI TORINO

Master's Degree in Civil Engineering

Master Thesis

EVOLUTIONARY ANALYSIS OF THE FRACTURING PROCESS IN MASONRY ARCHES:

APPLICATION OF THE COHESIVE CRACK MODEL

Tutors

Prof. Alberto CARPINTERI

Ing. Federico ACCORNERO

Candidate

Bartolo QUITADAMO

Academic Year 2018-2019

“This thesis is the result of hard work and a path full of obstacles. His conclusion is the result of the closeness of my family and of my girlfriend, Enza.

Thanks also to my Co-Tutor, Prof. Eng. Federico Accornero and to my employer Eng. Piergiorgio Venturella.”

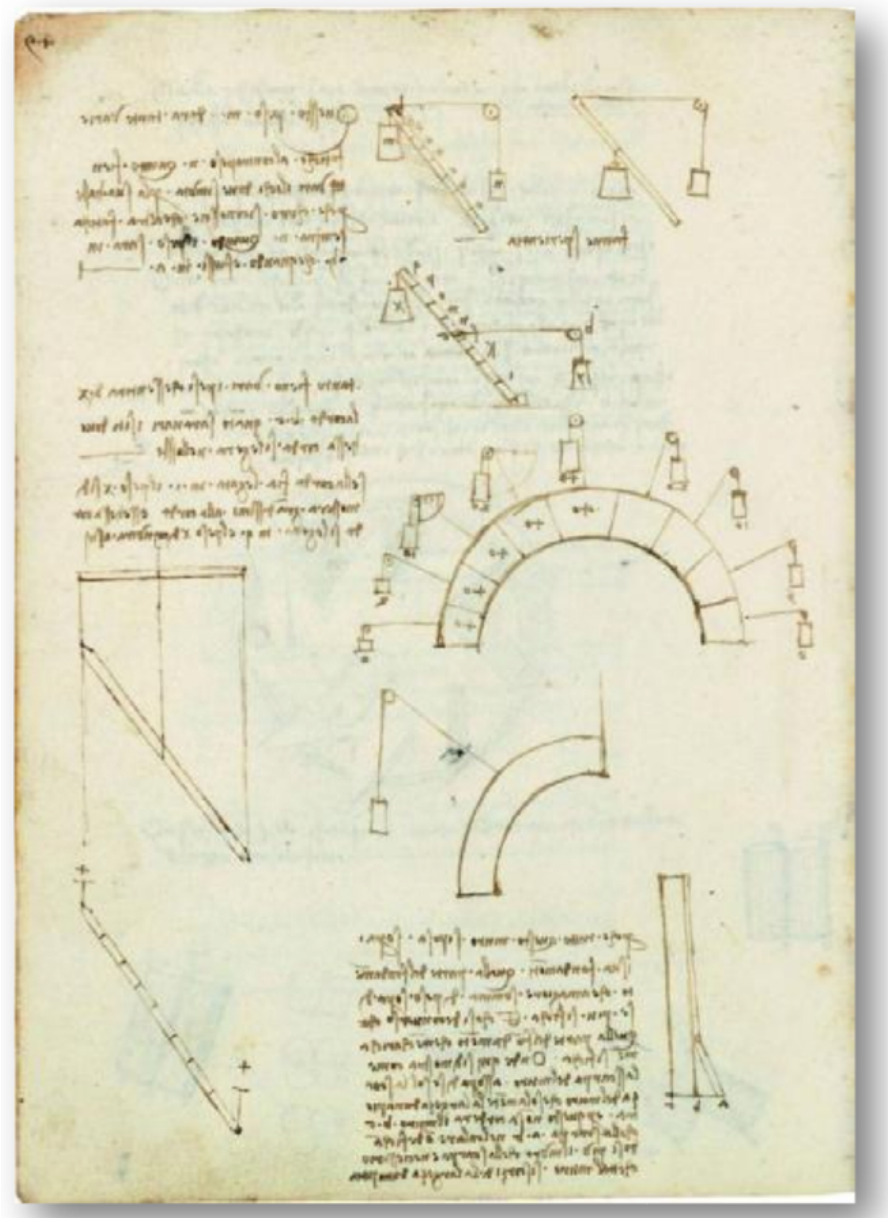

"L'arco non è altro che una fortezza causata da due debolezze imperochè l'arco negli edifici è composto di due quarti di circulo, i quali quarti circuli ciascuno debolissimo per sé desidera cadere e oponendosi alla ruina l'uno dell'altro, le due debolezze si convertono in un'unica fortezza"

(Leonardo da Vinci)

Table of contents

Abstract

In the present contribution, the Cohesive Crack Model was applied to the masonry arches. The model used is an elasto-plastic model able to coherently describe the behaviour of materials as it uses a couple of constitutive laws:

- A tension - strain relationship, which describes the elastic and hardening behaviour of the integral material up to the ultimate tension σ_u;
- A tension - opening of the slot relationship, which describes the "*softening*" behaviour of the cracked material, up to the critical opening w_c, in addition to which the interaction between the slit faces is annulated.

In the '80s an algorithm of calculation was developed, it was called "Frana", allowing it to apply the model of the cohesive crack to beam segments, simply supported, subject to simple bending moment. In the present work, the above mentioned algorithm has been translated into Matlab's language, after which it has been passed to adapt this model to the case of masonry arches. They may be considered as structures subject to off-centered compression.

To do this I used the theory of cohesive crack. In fact, the first part of the

constitutive law which describes the "softening" behaviour of the cracked material, has been translated in such a way that the tensile stresses due to the flexion were applied to a structure subjected to simple compression. The compression tension was considered equal to the compression tension produced in each section for the "arch’s effect".

The disordered and fragile materials such as concrete, rocks, ceramics and masonry contain a large number of defects and micro-cracks. By subjecting them to high tensile stresses, an interaction occurs between the growth processes of the micro-cracks which causes the localization of the deformation in a very narrow band, where the dissipation of energy occurs, while the material, outside this band, involves elastic and linear. According to the concepts of the continuous mechanics, it can be said that in this band (called the process zone), a reduction in load-bearing capacity occurs as a consequence of an increase in inelastic strain. This phenomenon is called a negative incrimination. The classical theory of plasticity is not applicable because the stability postulate of Drucker is violated. The consequences of this violation, even in the absence of geometrically unstable effects, are:

- possibility to have loss of stability in the crack opening control (snap-back);
- possibility to have loss of stability in displacement control (snap-through);

The algorithm developed identifies the section of the arch most stressed, in terms of tensile stress, that is, it identifies the section in which the crack will be created. At this point identify the load necessary for the crack to be born. In the following phases it identifies the load necessary for the increase to the crack.

The iteration ends when the height of the crack has reached to 90 percent of the total height of the section. At the same time, the algorithm performs a crushing check, that is, it evaluates, in the same section, if the maximum compression tension reaches to resistance of the material.

The cohesive crack model it was applied to 5 fictitious arches and to the Mosca bridge.

The analysis carried out allowed to show very interested results. In fact, plotting the increase in variable load with the relative vertical displacement of the section where are localized the brittle hinges, in control of amplitude of the crack, we obtain:

- loss of stability in the crack opening control (snap-back).

Wanting to chart the increase in load, obtained to propagate the cracks in the brittle hinges, with the absolute vertical displacement of the arch, measured in the arch crown, we obtain:

- loss of stability in displacement control (snap-through);

Therefore, in the sections in which the cracking progresses (local analysis), the unstable snap-back phenomenon is observed, while always during the cracking phase the arch (global analysis) shows a snap-through phenomenon.

Remember that the snap-back represents a phenomenon that can be framed within the framework of the Catastrophe Theory.

A further interesting result that has been found is that, for geometries with lower falls than 1/5 the cracking phenomenon does not develop. Moreover, the algorithm shows how, in the gradation of the degree of lowering, the second

pair of hinges is formed closer and closer to the arch crown (in fact, it passes from the arch behaviour to the beam behaviour).

1 Introduction

This thesis work deals with the use of the Cohesive Crack Model in the analysis of crack propagation problem in mode I in masonry arch.

When brittle materials are subjected to high tensile stresses, the interaction yaking place between the growth processes of the micro-cracks gives rise to a non linear type of behaviour. Energy dissipation occurs solely along a zone, referred to as the process zone, where the deformation is localised. The material outside this band retains its linear elastic behaviour. The behaviour of the material in the process zone is characterised by a reduction in bearing capacity due to an anelastic increment of Drucker's stability postulate ($d\varepsilon \geq 0$) which makes it impossible to apply ther Theory of Plasticity. This violation gives rise to phenomena such as loss of stability in controlled loading conditions (snap-through), loss of stability in controlled displacement conditions (snap-back), bifurcation of the equilibrium path and variability of the results depending on thr type of mesh employed in the numerical simulation. All this can be identified, as will be seen in the following chapters, applying the Cohesive Crack Model.

The Cohesive Crack Model uses two constitutive laws: one for the uncracked material and another that is applicable to the process zone. The first law is the

well known (definite positive) linear elastic relationship between stresses and strains, whilst the other is still a linear elastic law but has a negative slope and established a correlation between re-closing stresses and the mutual opening displacement in the process zone. In this way the Cohesive Crack Model manages to replicate the real behavior of the material in the cracking process.

The Finite Element Method had made to implement the foregoig consideration in a computation code and apply it to masonry arches.

2 Masonry bridges

2.1 Historical Overview

Archaeologists believe that arches and vaults originated in the marshlands of Lower Egypt or Mesopotamia about five thousand years ago. The prototype was a structure built of bundles of reeds placed upright in the ground and bent over and tied together at the top to form a roof. This technique is still used in southern Iraq. The outer surfaces of some of these buildings are covered with mud plaster and this was probably an intermediate stage in the evolution of the vault. Probably the Chinese first employed the arch in the construction of bridges across small streams. It is known that bridges and other public works were built there about 2900 BC and that possibly the arch was used then.

Nevertheless, the greatest examples of their use were the arch bridges built in the Roman age. Anyone approaching the study of masonry arch bridges will be struck by the diversity of structural models and materials employed in the Roman solution of bridging a gap with an arch. Many of them still exist and some remain in service to this day, together with the considerable number of masonry arch bridges built during the centuries until the First World War.

Figure 1 – Roman Bridge in Rome (Garibaldi Bridge)

The fundamental form of masonry bridges was surprisingly constant throughout the civilised world from Roman times through Byzantium and the Islamic world and into medieval Europe, where the church kept the secrets of masonry bridges alive. In fact, church building and bridge building were closely connected, with the same masons building both and travelling round Europe with the skills and secrets. St. Benezet who built the bridge at Avignon is well known, and the Pope was head of bridge building faculty of monks, and is thus still known as the Pontifex Maximus (Pontif) or chief bridge builder. It is interesting to note that in areas of strong nonconformist religion there were few masonry arches in the 18th century and early 19th century. The USA is surprisingly short of early masonry aches. This perhaps also accounts for the number of dramatic bridges could "Devil's Bridge", in that anything not buildable by the local church masons must have been built by the devil rather than the Romans, medieval monks or Moorish engineers.

The Age of Enlightenment and the scientific approach to bridge design started with the Italian Renaissance of the 15th century, which gave us the chain arch bridge and the segmental arch. But it became established in France in the 18th century with Hubert Gautier's Traite des Ponts published in 1716 and the formation of the Ecole des Ponts et Chaussees in 1747, which gave us balanced thrust arches.

This also led later to the separation of appearance from constructional necessity. In the 19th and 20th centuries the Ecole des Pontes et Chaussees advocated that the principles of masonry arch appearance should apply even if the structure underneath was not masonry. This Beaux Arts view, which was so in conflict with Modernism, probably hastened the separation of engineers from training in aesthetics, and promoted the idea of bridges being solely about pure engineering, and the false argument that "the appearance will look after itself if the structure is functional". Hitler's fondness for masonry arches on early autobahns probably aided their rejection post-war.

2.2 Description of the constructin method

There are two fundamental structural problems when building with masonry: how to achieve height and how to span an opening, i.e. how to span vertical and horizontal spaces. Spanning vertically is done by using columns, walls and towers, and spanning horizontally is done by using lintels, beams and arches. In addition, some structural elements such as vaults and domes can simultaneously span vertically and horizontally.

The arch is one of the older forms of bridge. It is rather like an inverted suspension bridge, with all the tensions replaced by compressions.

Masonry arches, being made of relatively big voussoirs joined by mortar cannot take tension and need continuous support during construction from below. This type of falsework is called centring, and is often of the general form shown below.

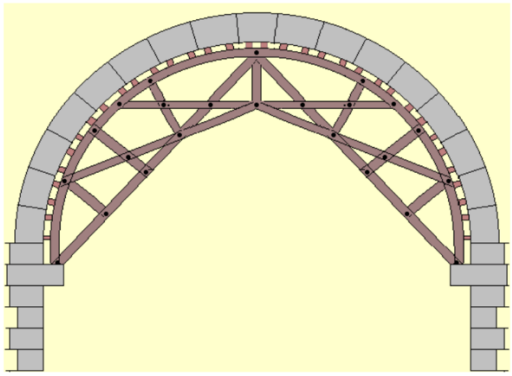

Figure 2 - Centring

The type of falsework depends very much on the material of which the bridge is made, and on the size of the bridge. This picture shows the corbels upon which the centring was erected.

When the centring has been removed, or struck, the arch will inevitably settle slightly. This is inevitable, because it can only generate the required compressive forces by undergoing some strain. All structures, in fact, must deflect when temporary support is removed.

The wedge shaped blocks from which an arch is built are known as voussoirs. They are usually symmetrically disposed about a central voussoir known as the

key-stone from a mistaken idea on the pat of early builders that it had a special function to perform. It is in fact an aesthetic and traditional feature rather than a structural requirement. The blocks in the abutments upon which the end of the voussoirs rest are known as skew backs and the surface between an end voussoir and a skew-back is the springing. The highest point of the arch is the crown and the lower sections are the haunches. This is a general term and there is no hard and fast definition of how much of the structure is included in a haunch. The upper boundary line of the arch ring is the extrados and the lower line is the intrados. The under surface of the arch ring is the soffit. The outer walls which retain the fill are the spandrel walls and they become the wing-walls at either side of the arch.

2.3 Design methods

2.3.1 Introduction

Over the centuries, different critical approaches have been used to address the problem of masonry arch design methods. These approaches are briefly described in chronological order, in the following paragraphs, to show how the partial understanding of arch structural behavior, as can be acquired from traditional methods, might be effectively improved.

2.3.2 Geometric and empirical design

For several centuries, methods that relied exclusively on geometric parameters were used to provide dimension to vaulted structures. If, on the one hand, such

methods originated from experience and provided an answer to the static problem, on the other, they neglected the intrinsic mechanisms forming the basis of the phenomena observed (Figure 3).

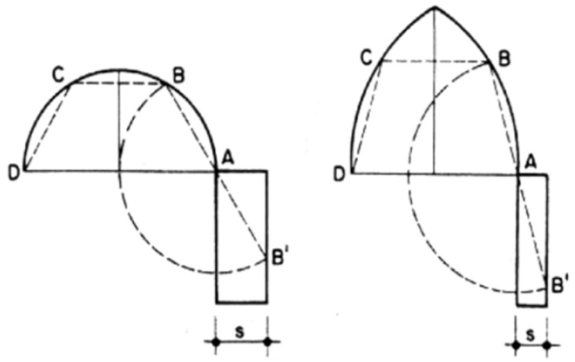

Figure 3 – Empirical formula for arch design: $\overline{\mathbf{AB}} = \overline{\mathbf{BC}} = \overline{\mathbf{CD}} = \overline{\mathbf{AB'}}$ (adapted from Vittone 1776)

Among the empirical approaches, we have to recall the statement given by Robert Hooke in 1675, who, at the end of his treatise on helioscopes, wrote: "Ut pendet continuum flexile, sic stabit contiguum rigidum inversum," which translates as, "As hangs the flexible line, so but inverted will stand the rigid arch" (Figure 4a). This sentence, originally written as an anagram, generalizes the idea of the funicular shape that a string takes under a set of loads. If rigidified and inverted, this shape illustrates a path of compressive forces for an arched structure to support the same set of inverted loads. This shape of the string and the inverted arch is called a funicular shape for these loads.

In 1748, Poleni analyzed a real structure using Hooke's idea to assess the safety of the cracked dome of St. Peter's in Rome. Poleni showed that the dome was safe by employing the hanging chain principle. For this, he divided the dome in slices and hung 32 unequal weights proportional to the weight of

corresponding sections of that "arch" wedge, and then showed that the hanging chain could fit within the section of the arch (Figure 4b). If a line of force can be found that lies everywhere within the masonry, then the structure can be shown to be safe for that set of loads [Heyman 1966].

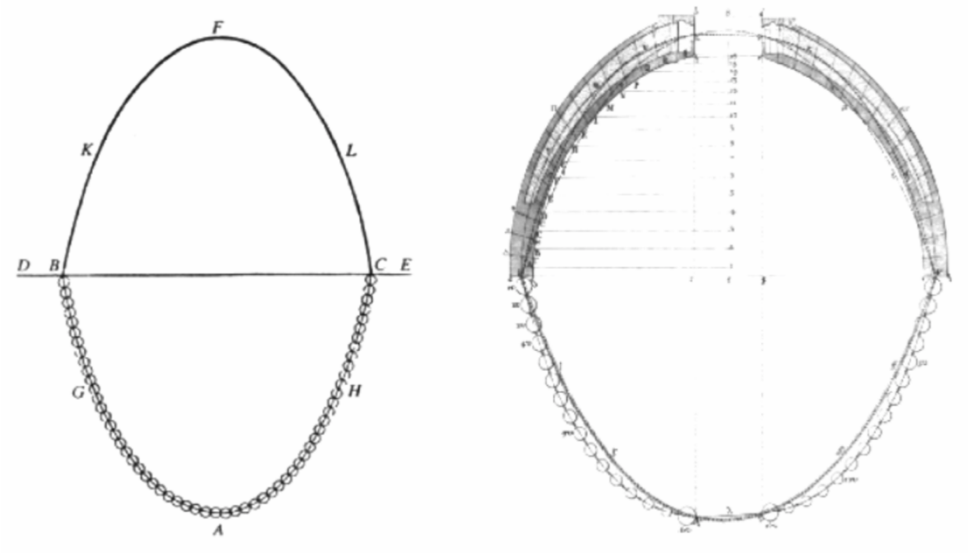

Figure 4 – (a) Poleni's drawing of Hooke's analogy between an arch and a hanging chain, and (b) his analysis of the Dome of St.-Peter's in Rome [1748].

2.3.3 Early kinematic Approch

In the eighteenth century, design, as it is meant today, saw the light, thanks to De La Hire (1730) and Mascheroni (1785), among others, who performed theoretical analyses and experimental tests to assess the state of an arch at final collapse. The developed design philosophy is close to the notions underlying both modern limit state and plastic design (Figure 5).

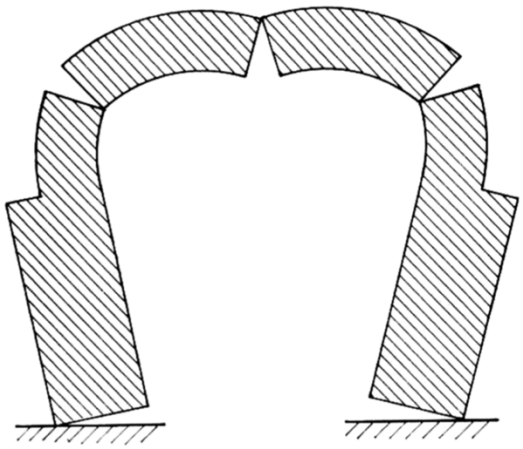

Figure 5 – Collapse mechanism according to Mascheroni

A significant contribution to the developing of De La Hire's topics was provided by Claude Antonie Couplet. He introduced the concepts of engrenèment entre les voussoir, that is, adherence and friction, which prevent the sliding along joints, and charnières, that is, the hinges whose formation allows the mutual rotation of the blocks [Couplet 1731]. Couplet's work, albeit little known among his contemporaries, has the great merit of expressing an outstanding progression in the theoretical setting of structural mechanics.

It is quite singular to note that the contribution given by Couplet was almost ignored in the following years. In fact, in 1773 Coulomb presented to the French Royal Academy the concepts of friction and hinge between arch blocks as absolutely original aspects. Coulomb developed a consistent and general theory providing the mathematical base for the description of the different possible modes of collapse, taking into account both relative rotations and sliding between parts. He also stated that the failure due to sliding is rare and suggested to consider only overturning (rotational) failures for practical

purposes. He proposed the use of a theory of "maxima and minima" (from our modern point of view, and optimization method) to determine the position of the more unfavourable hinges or sections of rupture.

A further development arrived with the thrust line theory and graphic statics during 19th c. Graphic statics supplied a practical method consistently based on the catenary principle. Graphic statics was actually used for the assessment of a large amount of masonry bridges and large buildings up to the beginning of 20th c. An example is given by Rubio's analysis of the structure of Mallorca Cathedral.

2.3.4 Elastic analysis

Navier (1833) was the first to observe the distribution of stresses at the interfaces between arch segments accurately. He shifted the focus of the analysis to the actual state of stress in the material. To analyze stress distribution over a cross section, he introduced the thrust-line concept. He also proved that the resulting line of action must lie within the central kern to prevent tension [Navier 1833].

Mery's (1840) studies gained widespread recognition. They were extensively used in the dimensioning of arch structures. His method was based on the use of a graphing procedure to check the thrust line in agreement with the stress limitations identified by Navier [Mery 1840]. Mery's method, successfully applied for over a century, is based on the following hypotheses:

- The analyzed arch is round and of constant thickness;
- The mechanism of breakage of Mascheroni (Figure 5) is valid, ie

formation of 3 plastic hinges, which 2 of on the kidneys and 1 in arch crown;

- The arch must have not excessive light (no more than 10 m);
- The arch must be constructed of approximate homogeneous material to a rigid body;
- The acting loads must be symmetrical with respect to the symmetry axis.

Furthermore this is a method of verification of breakage of the arches based on static graphics. Basically, when checking using this method, reference is made to an arbitrary line of pressures that passes to the key and the intrados to the kidneys and it is required that wherever it is contained within the middle third of the section (it is carried out the section only for a section of the arc that goes from the arch crown to the section to the kidneys). If the pressure curve remains within the average third-party strip, then all the sections are subject to compression and therefore the arch is stable. Therefore a collapse mechanism is assumed and a safety factor of 3 is required (ratio between the middle third and the whole thickness).

Soon, the application of the theory of elasticity encountered criticism: The concepts of homogeneity and isotropy, in fact, were far from the real conditions of damaged and cracked materials.

Alberto Castigliano (1879) tackled the problem by applying the minimum strain energy theorem to masonry arches. He also introduced the concept of an elastically imperfect system: "*Les corps qui, après avoir _et_e comprim_es, ne reprennent pas exactement leur formes primitives en enlevants les forces ext_erieurs.*"

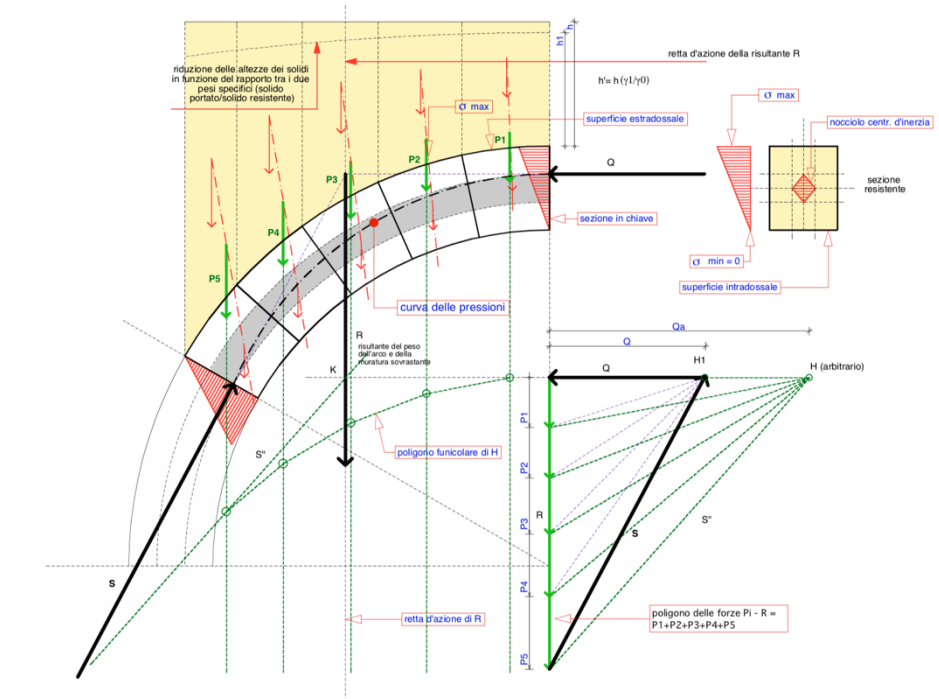

Figure 6 - Graphic method of Navier - Mery (1928). Stability verification of a symmetrical and symmetrically loaded arch.

2.3.5 Modern kinematic approach (Limit analysis)

The rigid-block model used in the eighteenth century to study the behavior of masonry arches underwent major revisions during the last century as a result of the various experiments carried out on arch models. One of the most significant revisions with respect to the eighteenth-century theories was formulated by Heyman (1966, 1982). Referring back to Kooharian's (1953) studies, he proposed that plastic theory formulated initially for steel structures could be applied to masonry gravity structures such as arch bridges provided certain assumptions were made. An underlying premise was that masonry can conceptually be considered as possessing a 'ductile' moment capacity, albeit one which is primarily a function of the arch thickness and normal force at a

cross-section.

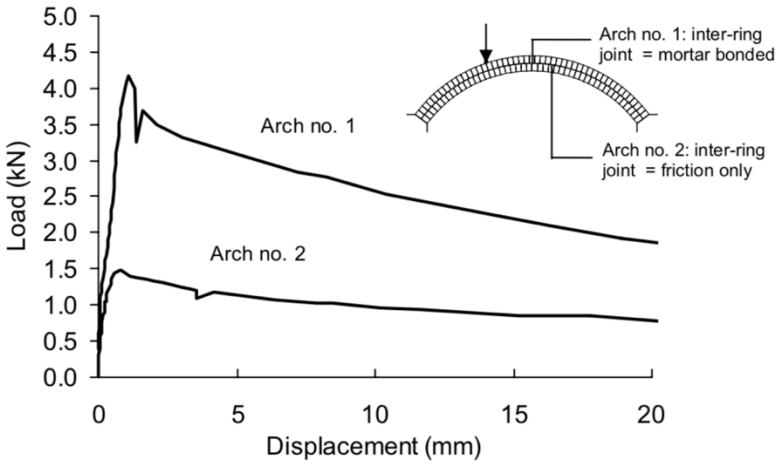

Figure 7 – Load – deflection responses of two 3 m span brickwork arch ribs (after Gilbert 1997).

Experimental evidence largely supports this standpoint. For example Figure 7 shows the load vs. deflection responses of two bare masonry arch ribs of differing construction tested to collapse in the laboratory. Using terminology borrowed from the field of steel structures, in both cases it is evident that the overall response is reasonably "ductile" (in that the fall off in capacity is relatively modest providing displacements are small). The contribution of interring friction to the resistance in the case of arch no. 2 increases this apparent "ductility". Similarly when soil filling is present the response generally becomes yet more "ductile", as increasing mobilized soil strength acts to counteract the damaging effects of gross displacements. Thus Heyman strongly argued that plastic theory should also be applied to the analysis of masonry structures, including masonry arch bridges specifically [Heyman 1980]. To perform an analysis he simplified the problem by assuming that:

1. stone has no tensile strength;
2. stone has infinite compressive strength;
3. the sliding of a stone on another cannot occur.

The choice of this constitutive law for the material, however, seems to be penalizing compared to the way the material actually behaves. In fact, although it may be true that the shear component of the stress, exerted between two adjacent voussoirs, cannot by any means exceed the friction resistance, the fact remains that stone is considered as a material with no tensile strength but infinite compressive strength.

Starting from these assumptions, the formation of a hinge right where the thrust line is tangent to the arch at the edges can be acknowledged; thus, a rigid rotation of the faces of the two adjacent segments takes place around the extreme fiber of the section [Gilbert and Melbourne 1994].

Three tangential points lead to the formation of three hinges; this results in a statically determinate structure. The limit to trigger a kinematic collapse mechanism lies in the formation of a fourth hinge. The limit analysis consists of the identification of the lowest possible load multiplier that generates a line of thrust that is always contained within the arch volume and tangential to arch edges at four points (hinges) (Figure 8).

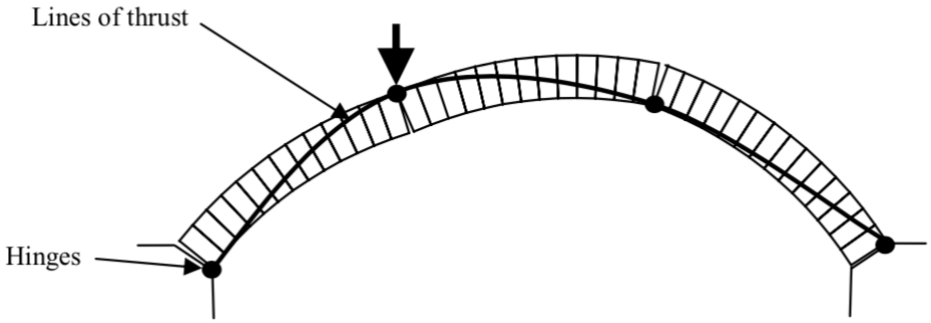

Figure 8 – Thrust line at collapse in masonry arch.

The theorems of plastic limit analysis require satisfaction of certain conditions [Horne 1979] and before proceeding further it is worthwhile to simply state these:

I. Equilibrium condition The computed internal actions must represent a state of equilibrium between the internal and external loads (the corollary of the equilibrium conditions are compatibility conditions, which should instead be satisfied if an energy method is being used).
II. Mechanism condition Sufficient releases must be made to transform the structure into a mechanism.
III. Yield condition. The stresses in the material must be everywhere less than or equal to the material strength (e.g. shear, crushing and tensile strength limits must all be respected).

Now consider a structure subject to an applied load which is multiplied by a load factor λ. The three fundamental theorems of plastic analysis can now be stated in simplified form as:

- Static or lower bound theorem If at any load factor λ the equilibrium and yield conditions are everywhere satisfied, then $\lambda = \lambda_I$ which is less than or equal to the failure load factor λ_p.
- Kinematic or upper bound theorem If at any load factor λ is equal to the work done in plastic energy dissipation, then $\lambda = \lambda_u$ which is greater than or equal to the failure load factor λ_p.
- Uniqueness theorem If at any load factor λ, the internal stress state is such that the three conditions of equilibrium, mechanism, and yield are satisfied then that load factor is the collapse load factor λ_p.

The relationship between upper and lower bound solutions is also presented graphically in Figure 9 below.

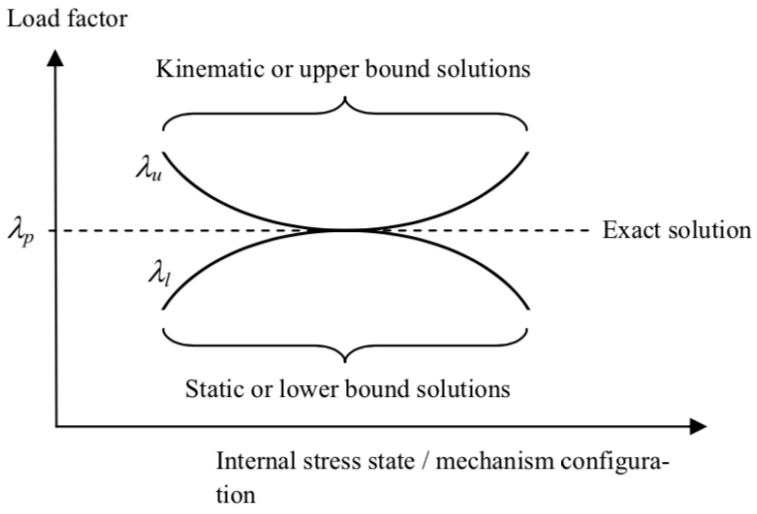

Figure 9 – The relationship between upper and lower bound solutions.

Figure 9 also provides an indication that optimization techniques can be applied

to search for the exact solution, corresponding to the exact load factor λ_p. Such techniques will be discussed later in the paper.

Heyman considered only the hinging or "rocking" yield condition, excluding the possibility of sliding or crushing failure. This meant that for the lower bound theorem to be satisfied all that was required was for a thrust line to be identified which was in equilibrium with the applied loads, and which lay wholly within the masonry.

Linked to the above theorem, Heyman then proposed the concept of a geometric factor of safety (G.F.O.S.), which gives an indication of how much larger the arch under consideration is in comparison to one that is just stable under the given loading pattern. One advantage of the G.F.O.S. is that it can be applied to long span bridges where foreseeable live loads may be neg- ligible in comparison to structural self weight.

Harvey (1988) extended the applicability of Heyman's "safe theorem" and G.F.O.S. by proposing that the term 'thrust line' be replaced with 'thrust zone', which at each cross-section is of sufficient depth to carry the load, based on consideration of the actual material crushing strength.

2.3.6 Recent developments (FEM analysis)

Extensive studies have been carried out recently on arch and vault structures, some of them dealing with the problem of friction resistance. Several studies based on the finite-element method (FEM) and on nonlinear FEM tension models show the potential of the method to compute both load-deflection curves and the interaction of the arch structure with the filling.

Most of modern possibilities based on FEM fall within two main approaches referred to as macro-modelling and micro-modelling.

2.3.6.1 FEM Based approaches. Macro-Modelling

Macro-modelling is probably the most popular and common approach due to its lesser calculation demands. In practice-oriented analyses on large structural members or full structures, a detailed description of the interaction between units and mortar may not be necessary. In these cases, *macro-modelling,* which does not make any distinction between units and joints, may offer an adequate approach to the characterization of the structural response. The macro-modelling strategy regards the material as a fictitious homo- geneous orthotropic continuum.

An appropriate relationship is established between aver- age masonry strains and average masonry stresses. A complete macro-model must account for different tensile and compressive strengths along the material axes as well as different inelastic properties along each material axis. The continuum parameters must be determined by means of tests on specimens of sufficiently large size subjected to homogeneous states of stress. As an alternative to difficult experimental tests, it is possible to assess experimentally the individual components and consider the obtained data as input parameters of a numerical homogenization technique. Compared to more detailed approaches affording the description of discontinuities, macro-modelling shows significant practical advantages. In particular, FE meshes are simpler since they do not have to accurately describe the internal structure of masonry and the finite elements can have dimensions greater than the single brick units. This type of modelling

is most valuable when a compromise between accuracy and efficiency is needed.

The macro-models, also termed *Continuum Mechanics finite element models*, can be related to plasticity or damage constitutive laws.

The macro-models have been extensively used with the aim of analyzing the seismic response of complex masonry structures, such as arch bridges (Pela' et al.), historical buildings (Mallardo et al.), and mosques and cathedrals (Roca et al., Martínez et al.; Murcia-Delso et al.).

A drawback of the macro-modelling approach lays in its description of damage as a smeared property spreading over a large volume of the structure. In real unreinforced masonry structures, damage appears normally localized in isolate large cracks or similar concentrated lesions. A smeared modelling of damage provides a rather unrealistic description of damage and may result in predictions either inaccurate or difficult to associate with real observations.

Macro-models encounter a significant limitation in their inability to simulate strong discontinuities between different blocks or parts of the masonry construction. Such discontinuities, corresponding either to physical joints or individual cracks formed later in the structure, may experience phenomena such as block separation, rotation or frictional sliding which are not easily describable by means of a FEM approach strictly based on continuum mechanics.

However, a possible way of overcoming these limitations consists of the inclusion within the FEM mesh of joint interface-elements to model the response of discontinuities.

2.3.6.2 FEM Based approaches. Micro-Modelling

n the micro-modelling strategy, the different components, namely the units, mortar and the unit/mortar interface are distinctly described. The socalled *detailed* micro-models describe the units and the mortar at joints using continuum finite elements, whereas the unitmortar interface is represented by discontinuous elements accounting for potential crack or slip planes (Figure 10). Detailed micro-modelling is probably the more accurate tool available to simulate the real behavior of masonry. It is particularly adequate to describe the local response of the material. Elastic and inelastic properties of both unit and mortar can be realistically taken into account.

The detailed macro-modelling strategy leads to very accurate results, but requires an intensive computational effort. This drawback is partially overcome by the *simplified* micro-models, where expanded units, represented by continuum elements, are used to model both units and mortar material, while the behavior of the mortar joints and unitmortar interfaces is lumped to the discontinuous elements (Figure 10). Masonry is thus considered as a set of elastic blocks bonded by potential fracture/slip lines at the joints.

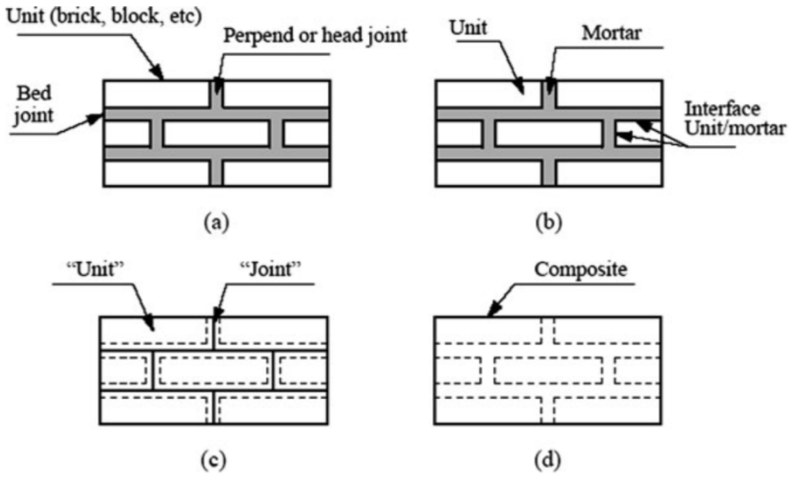

Figure 10 - Modelling strategies for masonry structures (Lourenço): masonry sample (**a**); detailed (**b**) and simplified (**c**) micro-modelling; macro-modelling (**d**)

The micro-modelling approaches are suitable for small structural elements with particular interest in strongly heterogeneous states of stress and strain. The primary aim is to closely represent masonry based on the knowledge of the properties of each constituent and the interface. The necessary experimental data must be obtained from laboratory

tests on the constituents and small masonry samples. Nevertheless, the high level of refinement required means an intensive computational effort (i.e. great number of degrees of freedom of the numerical model), which limits micro-models applicability to the analysis of small elements (as laboratory specimens) or small structural details.

2.3.7 LEFM Model for masonry arches

2.3.7.1 Introduction to fracturing process

More recent methods [Carpinteri et al. 2015; Accornero et al. 2016; Lacidogna and Accornero 2018] for the evaluation of masonry arch structure stability consist of incremental analysis of the fracturing process by means of LEFM.

Masonry is characterized by anisotropic and nonlinear behavior even at low strain values. Masonry materials subject to uniaxial load tests exhibit appreciably different tensile strength and compressive strength values: the latter being significantly higher than the former. Therefore it was thought that the constitutive law that best represents the behavior of natural or artificial masonry materials is an elastic-softening constitutive law (Figure 11). This is equivalent to simply considering an elastic constitutive law combined with a crisis condition for fracturing in accordance with the concepts of LEFM; that is to say, the material has a purely elastic behavior with the possibility of cracks forming and propagating.

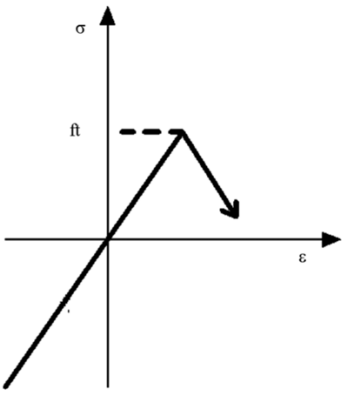

Figure 11 – Elastic-softening constitutive law.

2.3.7.2 Mechanism of crack opening and closure

At the base of this method there is the hypothesis that, an elastic-softening material is replaced by a material with a purely elastic behavior with the possibility of cracks formation and extension. This hypothesis applies only to structures large enough to allow tension profiles to develop close to the crack tip, as foreseen by linear elastic fracture mechanics.

Take normalized crack depth ξ = a/b (Figure 12.a) as the damage parameter and the stress intensity factor, K_I, (Figure 12.b) as the load parameter. The stress intensity factor is an amplification factor of the stress field when the loads are symmetrical relative to the crack (e.g., axial force and bending moment). Shear is disregarded.

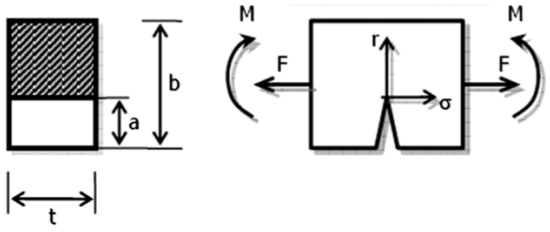

Figure 12 – Cracked beam element: $\boldsymbol{\xi = ab^{-1}}$; $\boldsymbol{\sigma = K_I(2\pi r)^{-0.5}}$

The energetic meaning of K_I , the square of this parameter, omitting a proportionality factor, represents the elastic energy released by the system per unit of virtual crack extension. The K_I reaches its critical value K_{IC} when this virtual extension becomes real, since the energy released in an elementary crack extension is sufficient to supply the surface energy of the new geometry.

The bending moment produces a stress intensity factor at the crack tip

expressed as:

$$K_I = \frac{M}{tb^{3/2}} Y_M(\xi) \quad (1)$$

with:

$$Y_M(\xi) = 6\left(1.99\xi^{\frac{1}{2}} - 2.47\xi^{\frac{3}{2}} + 12.97\xi^{\frac{5}{2}} - 23.17\xi^{\frac{7}{2}} + 24.8\xi^{\frac{9}{2}}\right) \quad (2)$$

Similarly, a tensile axial force, F, produces:

$$K_I = \frac{F}{tb^{1/2}} Y_F(\xi) \quad (3)$$

with:

$$Y_F(\xi) = 1.99\xi^{\frac{1}{2}} - 0.41\xi^{\frac{3}{2}} + 18.70\xi^{\frac{5}{2}} - 38.50\xi^{\frac{7}{2}} + 53.86\xi^{\frac{9}{2}} \quad (4)$$

When the axial force is compressive and the bending moment tends to open the crack, as is usually the case in masonry arches, the total stress intensity factor can be determined by applying the superposition principle:

$$K_I = K_{IM} - K_{IF} = \frac{F}{tb^{1/2}}\left[\frac{e}{b} Y_M(\xi) - Y_F(\xi)\right] \quad (5)$$

where e stands for the eccentricity of the equivalent axial force, relative to the centroid of the cross-sectional area.

From the critical condition $K_I = K_{IC}$, it is possible to determine the dimensionless crack extension axial force as a function of crack depth ξ and relative eccentricity of the load, e=b:

$$\overline{F_C} = \frac{F_C}{tb^{1/2}K_{IC}} = \frac{1}{\frac{e}{b}Y_M(\xi) - Y_F(\xi)} \quad (6)$$

The curves in Figure 13 graphically represent this expression and show how, when eccentricity e=b is fixed, the fracturing process reaches a condition of stability only after showing an unstable condition. If the load F is unable to follow the decreasing unstable branch of the e= b = constant curve in a strain-softening unloading process, the fracturing process leads to catastrophic behavior and the representative point advances horizontally until it meets the e= b = constant curve again on the stable branch. On the other hand, the possibility of load relaxation and a more or less catastrophic fracturing behavior depends on the structure's geometric and mechanical characteristics and is affected in particular by degree of redundancy and size (scale effect).

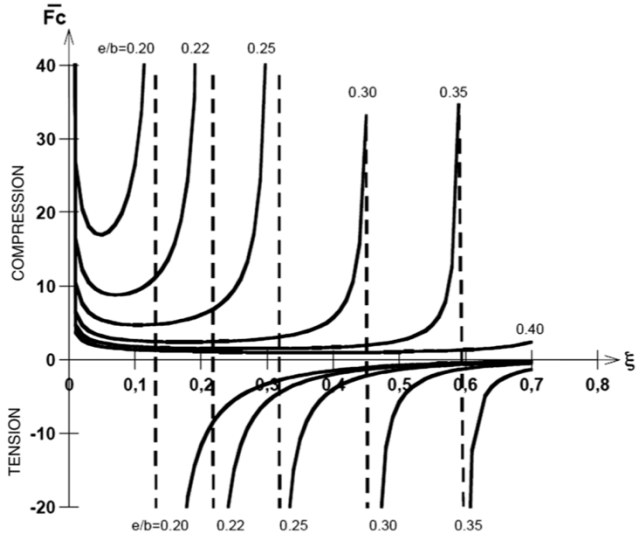

Figure 13 – Fracturing process for eccentric axial load.

It is also important to consider that, for each relative crack depth ξ, there is a relative eccentricity value below which the crack tends, at least partially, to close again. From the closing condition $K_I = 0$, the following is obtained:

$$K_I = 0 = \frac{F}{tb^{1/2}}\left[\frac{e}{b}Y_M(\xi) - Y_F(\xi)\right] \quad (7)$$

from which:

$$\frac{e}{b} = \frac{Y_F(\xi)}{Y_M(\xi)} \quad (8)$$

This equation is graphically represented in Figure 14. The area below the curve represents the crack and loading conditions whereby $K_I < 0$.

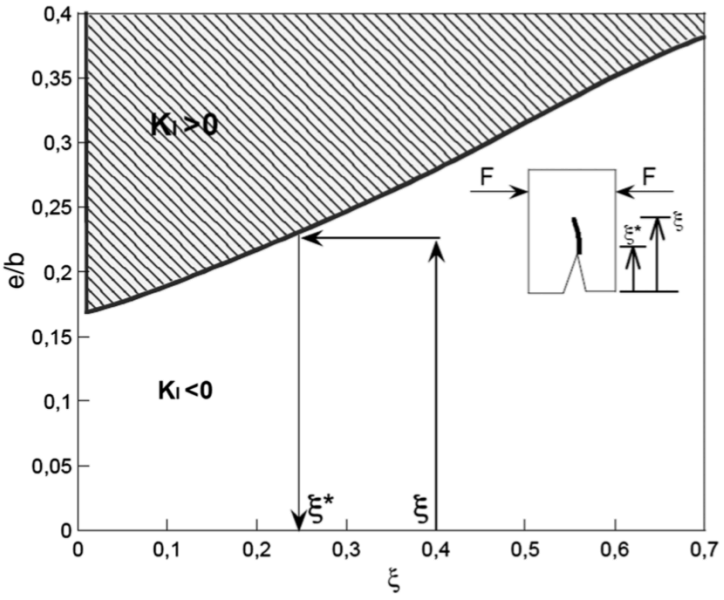

Figure 14 – Crack closuse curve

2.3.7.3 Stiffness of the cracked section

Now consider the loss of stiffness in the cross section of a cracked beam. A cracked cross section (Figure 12.a) behaves like an elastic hinge with the rotational stiffness determined by an energy balance between elastic work and fracture work.

The rotational stiffness of an elastically fixed joint is:

$$W = \frac{b^2 tE}{2\int_0^{\xi} {Y_M}^2(\xi)d\xi} \quad (9)$$

where E= Young's modulus of the material. The stiffness matrix of the cracked element (Figure 15) is changed only by the four rotational terms as described in Figure 16, where A and I are the area and the inertia moment of the cross section, respectively, and l is the length of the beam finite element.

From the stiffness matrix, it can be seen that terms that link the moments M_1 and M_2 to the rotations ϕ_1 and ϕ_2 obtained by applying the principle of virtual work to a beam with an elastic hinge simulating a crack at the midspan, return the standard values of the uncracked beam finite element as W tends to infinity:

$$\lim_{W\to\infty} \varphi \frac{EI(3EI + 4lW)}{l(EI + lW)} = \varphi \frac{4EI}{l} \quad (10)$$

$$\lim_{W\to\infty} \varphi \frac{EI(3EI + 2lW)}{l(EI + lW)} = \varphi \frac{2EI}{l} \quad (11)$$

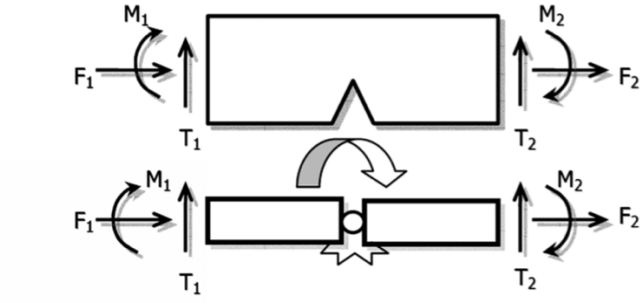

Figure 15 – Cracked beam elemnt: elastic hinge simulating a crack.

	u_1	v_1	φ_1	u_2	v_2	φ_2
F_1	$\frac{EA}{l}$	0	0	$-\frac{EA}{l}$	0	0
T_1		$12\frac{EI}{l^3}$	$-6\frac{EI}{l^2}$	0	$-12\frac{EI}{l^3}$	$-6\frac{EI}{l^2}$
M_1			$\frac{EI(3EI+4lW)}{l(EI+lW)}$	0	$6\frac{EI}{l^2}$	$\frac{EI(3EI+2lW)}{l(EI+lW)}$
F_2				$\frac{EA}{l}$	0	0
T_2		*symmetric*			$12\frac{EI}{l^3}$	$6\frac{EI}{l^2}$
M_2						$\frac{EI(3EI+4lW)}{l(EI+lW)}$

Figure 16 – Stiffness matrix of the cracked element.

2.3.7.4 Calculation procedure

Setting the geometrical characteristics of the structure and the mechanical characteristics of the material, like the maximum compressive stress and the fracture toughness K_{IC}, the arch is analyzed by creating a FEM (Finite Element

Method) model and considering the stone structure clamped to rigid abutments. The calculation uses a step-by-step loading process and for each load increment the code returns the axial force and bending moment in each section; from these values, using the classical relations of beam theory, it is possible to determine the maximum tensile or compressive forces and their eccentricity with respect to the centroid in each section of the structure.

When a section crisis is triggered by tensile stresses, the relative crack depth ξ is determined. In this way, the updated crack depth is determined.

Therefore, the routine is applied again considering the modified stiffness of the cracked elements. If the new relative crack depth ξ is equal to that formerly determined, the process stabilizes. If the new relative crack depth ξ is lower than the former, the routine resorts to the curve of closure, which allows to check the value of the stress intensity factor K_I, determining the admissible crack depth. After this check, the ξ values which fall in the field $K_I \geq 0$ are considered.

Increasing the load, the inefficiency of the arch section takes place when $\xi \geq 0.7$, or when the compressive strength in the considered element is reached.

3 The cohesive crack model

3.1 Fondation of the cohesive crack model

"*As is known, the intensity of the force of cohesion, actiong between two pieces of material previously constituting a single unit and afterwards separeted, depends strongly on thr distance y between these segments.*"[1]

This model was proposed by Barenblatt and Dugdale. He was later spotted by Bilby, Cottrell and Swinden, Willis and Rice. More recently it was re-proposed by Wnuk under the name of Final Stretch Model and by Hillerborg, Modeer and Petersson under the name Fictious Crack Model. Carpinteri re-proposed in 1985 the primitive name of Cohesive Crack Model.

The basic hypothesis is that, as extension of the real crack, a fictitious fissure, called "Process Zone", is formed in which the material, although damaged, is still able to transfer tensions.

[1] G.I. Barenblatt, "On some basic ideas of the theory of equilibrium crack …", 1961.

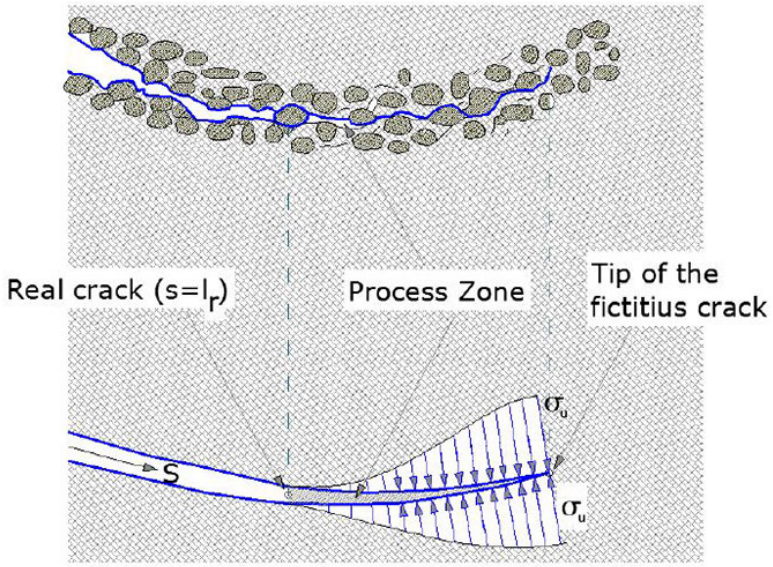

Figure 17 – Process zone (without shearing stresses).

In fact, according to the theory of elasticity, described in Paragraph 2.3.7, at the apex of a crack, there is a stress singularity. In practice, the materials solicited beyond the limit of proportionality exhibit non-linear behavior. This means that, around the end of the crack, there is always a non-linear behavior zone and therefore the stress singularity disappears. The cohesive model allows us to grasp and take into account this non-linear behavior. From the standpoint of non-linear behavior, one can essentially distinguish two types of materials:

1. Some materials, if deformed beyond the limit of proportionality, have further resistance reserves and are called "strain hardering". In these cases, energy dissipation occurs mainly in the volume of the material, in a plastic area located around the apex of the crack. In this family of materials are mainly those of metal.

2. Other materials, if deformed beyond the limit of proportionality, show a decrease in resistance which is also called "strain softening". In these cases, the non-linear zone tends to localize in a very narrow band collinear to the fissure. Energy dissipation occurs mainly on the surface of the fracture. This material family includes concrete, rocks, bricks, ceramics and fibro-reinforced compounds.

In this last case, the process zone can be simulated with a "cohesive force distribution" behind the end of the fictitious fissure, i.e. it can be studied with the cohesive model. In fact, this model is able to explain the transition between the two extreme situations of collapse:

a) that foreseen by the limit analysis, for the achievement of the last bending moment in the weakened section from the notch;
b) that foreseen by the Linear Elastic Fracture Mechanics, for fracture propagation.

3.2 The cohesive constitutive law

In the non-linear fracture model (cohesive model) the way to consistently describe the behavior of materials is to use a set of constitutive laws:

I. a tension-strain relationship, which describes the elastic and hardening behavior of the integral material up to the maximum tension (σ_u), including the drains (to see Figure 18a);
II. a tension-opening of the crack relationship, which describes the "softening" behavior of the cracked material, up to the critical opening

of the toilet, beyond which the iteration between the faces of the crack is canceled (to see Figure 18b).

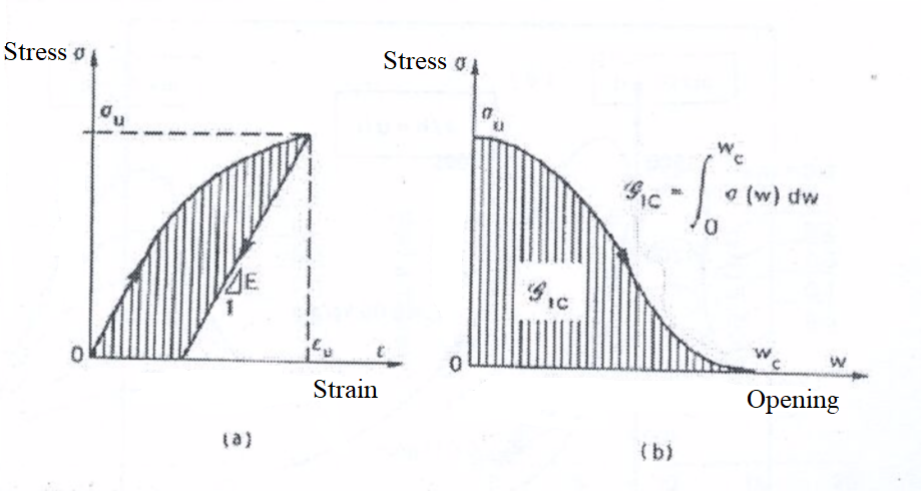

Figure 18 – Constitutive law: (a) undamaged material, (b) process zone.

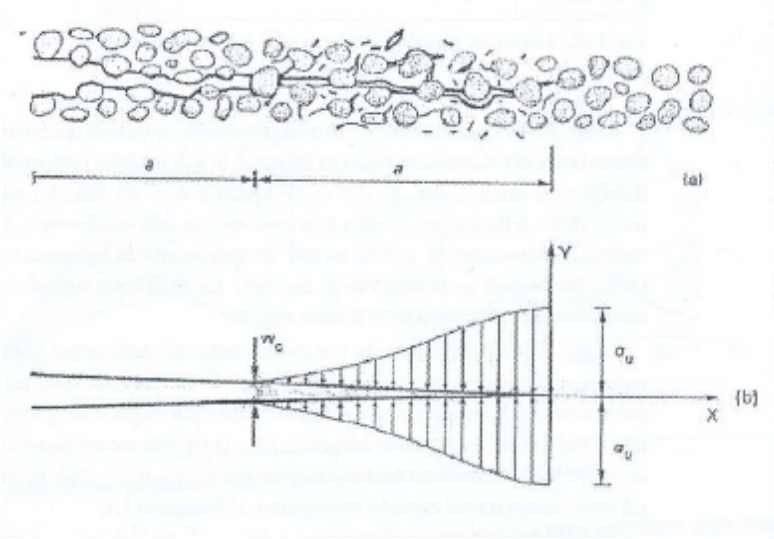

Figure 19 - The cohesive crack model: (a) Process zone; (b) Cohesive forces of reclosing.

For steels the constitutive law is generally of the most complex type, and a modeling is somewhat more difficult because it must provide two different dissipation mechanisms (dissipation in the volume of intact material and on the

surface of the crack), for concretes, rocks, walls (where the dissipation of energy takes place exclusively on the surface of the crack) the simplest elasto-softening law is able to coherently describe reality.

The so-called cohesive crack model is quite similar to the Dugdale model but, unlike the latter, the distribution of cohesive forces is not constant but decreases as the crack opening increases, with a softening law (Figure 18b). The area facing the end of the "real" crack is damaged and micro-cracked and in it a segment of the macrofession in progress can be distinguished, still however partially sewed by inclusions, aggregates and fibers (Figure 18a). This zone, where non-linear and dissipated microscopic phenomena occur, as previously mentioned, takes the name of "Process zone".

The end of the cohesive (or fictitious) slot coincides with the end of the process zone, in which the opening w is canceled and the reclosing tension is equal to the tensile strength σ_u, this point takes the name of fictitious crack tip. The end of the real slot is instead located at the critical opening w_c, so the interaction is canceled, this point is called real crack tip. In the intermediate points of the process zone, the pairs σ-w are provided by the cohesive law (Figure 18b).

3.3 The cohesive model in problems of MODE I

The cohesive model is based on the following assumptions:

1) the process zone begins to develop when the maximum main tension reaches the tensile strength of the material;

2) the process zone is developed perpendicular to the main tensile tension;
3) in the process area the material is partially damaged, but can still transfer tensions. In numerical simulations, the process zone is represented as a fictitious extension of the crack.

The tensile forces, which act on the fictitious extension of the crack, are defined as decreasing functions of the distance w between the flap edges. About these forces, called cohesive, in the numerical simulations that will be present later, the following hypotheses have been assumed:

4) absence of tangential components;
5) σ-w linear law:

$$\sigma = \sigma_u \left(1 - \frac{w}{w_c}\right) \quad (12)$$

where w_c is the critical opening value of the crack, i.e. it is assumed that for opening values greater than w_c, the material is not able to transmit stress. The area subtended by the curve σ-w, represents the fracture energy $\mathcal{G}_F = \mathcal{G}_{IC}$.

6) w is an increasing monotone function of time during the irreversible cracking process;
7) outside the damaged area, the material behaves in an elastic-linear manner.

Based on the previous hypothesis, indicating with w(x) the opening of the crack in a generic point, and considering the reference system (Figure 19), we obtain:

$$\lim_{x \to 0^-} w = 0 \quad (13)$$

and taking into account the cohesive law:

$$\lim_{x\to 0^-} \sigma = \sigma_u \qquad (14)$$

This last formula indicates that, approaching the apex of the fictitious fissure along the process area, the tension tends to σ_u. The hypothesis 2) indicates that, under conditions of incipient propagation of the fissure, it results:

$$\lim_{x\to 0^+} \sigma = \sigma_u \qquad (15)$$

This equation indicates that, by approaching the apex of the fictitious fissure coming from the intact material and moving in the -x direction, the main tensile tension tends again to the value σ_u.

These last two equations show that $\sigma(x)$ is a continuous function in x= 0. The cohesive model does not involve the emergence of tension singularities and therefore the use of singular elements is not required.

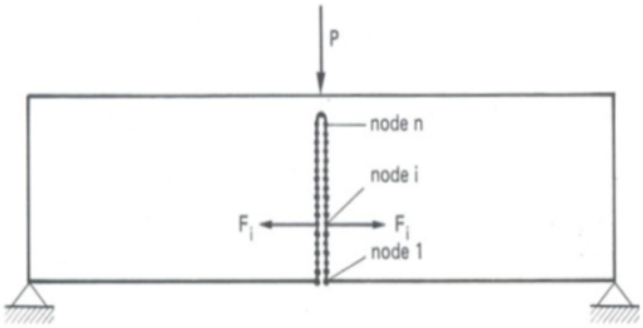

Figure 20 - Nodes of the lattice of finite elements placed at the crack propagation line.

In the problems of MODE 1, the crack trajectory is known for considerations of symmetry. Applying the Finite Element Method, it is possible to build a mesh with *n* pairs of nodes arranged along the direction of propagation of the crack.

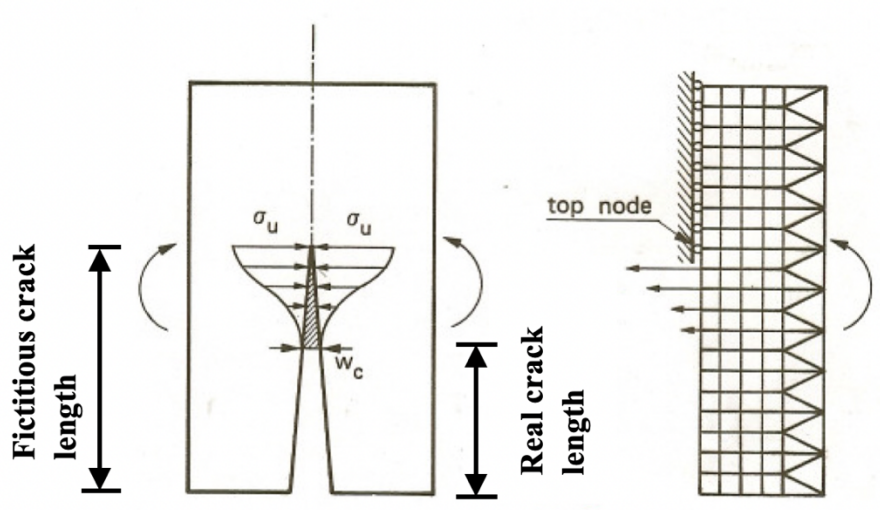

Figure 21 - Stress acting on the fictitious fissure. (a) and equivalent nodal forces applied to the lattice of finite elements.

Hence, the cohesive forces are rapresented by nodal forces, F_i, whose intensity depends on the opening of the crack according to the costitutive law of the material, σ_c-w_n.

The problem can be formulated as follow:

$$\{w\} = [H]\{F\} + \{C\}P \qquad (16)$$

where,

$\{w\}$= stands for the vector, of size *n,* containing the opening displacements of the crack;

[H]= is the matrix, of size *nxn,* of the influence coefficients corresponding to *Fj*= 1;

$\{C\}$= is the vector of the influence coefficients of the action due to the unit external load *P.*

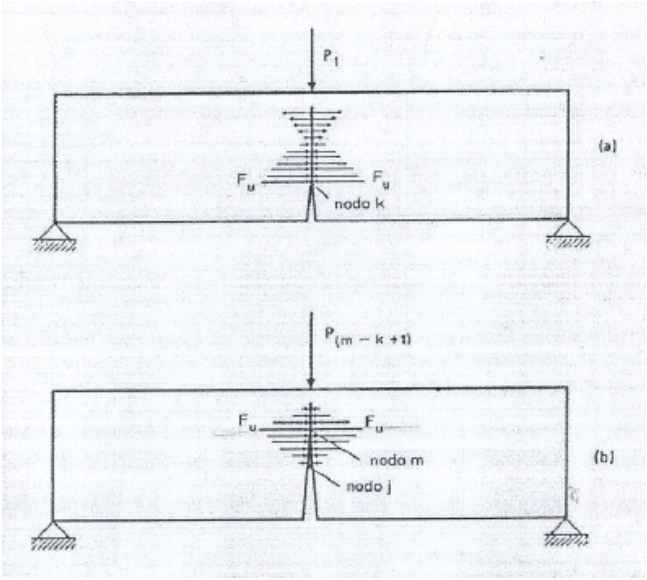

Figure 22 - Distribution of the forces of reclosing above the real crack tip, at the first step (a) and at a generic step (b) for advancing the crack.

The cohesive tensions of reclosing, acting on the fictitious crack (Figure 21a) are replaced by nodal forces (Figures 21b). The intensity of these forces depend, as said by the opening of the fissures w, according to the law σ-w. At a generic propagation step (Figures 22) one can then write the following equations:

$$F_i = 0; \quad \text{for i=1, 2 …, j-1;} \quad \text{real crack } (w > w_c); \qquad \textbf{(17.a)}$$

$$F_i = F_u\left(1 - \frac{w_i}{w_c}\right) + F_N \quad \text{for i= j, …, m-1;} \quad \text{fictitious crack } (0 < w < w_c); \qquad \textbf{(17.b)}$$

$$F_i = F_u \; and \; w_i = 0 \quad \text{for i= m;} \quad \text{tip of fictitious crack;} \qquad \textbf{(17.c)}$$

$$w_i = 0 \quad \text{for i= m+1, …, n;} \quad \text{uncracked material;} \qquad \textbf{(17.d)}$$

Where, F_N is the additional term that takes into account the presence of compression. F_N is a function of q.

The total number of equations is 2n+1 (n is the numner of Eqs. (16) and n+1 that of Eqs. (17.a-d)), as well as that of the unknowns, *w, F* and *P.*

The deflection of the loading point is determined by:

$$\delta = \{C\}^T\{F\} + D_p P \qquad (18)$$

where D_p denotes the deflection of the loading point when $P = 1$.

The equations in the system depend on the indices *j* (tip of the real crack) and *m* (tip of the fictitious crack), which vary with the crack propagation process. The instructions for determining such equations are as follows:

1) At the first step the process zone has not yet been formed and the real crack tip coincides with the tip of the notch, so that j = m. When there is no notch, then m=j=1;
2) At each step, the fictitious crack increases by a quantity *fly* so that *m* is increased by 1;
3) Solve the system of 2n + 1 equations and check the opening w_j of the tip of the real crack:
    a. If $w_c \geq w_j$: go to step 4);
    b. If $w_j > w_c$: increase j and check the remaining number of cohesive links (which is m - j):
        i. $m - j \geq 4$: the system is well posed, return to step 3);
        ii. m - j < 4: the problemi s too brittle. Refine thr mesh (by increasing n) and repeat the analysis;

4) Make sure that $F_i < F_u$ in the uncracked material and that $w < w_c$ in the orocess zone;
5) Determine the deflection δ of the loading point on the basis of Eq. (18).
6) If m < n go back ti spet 2); if it is not, the analysis stops.

In elastic and elasto-plastic models, the stress and displacement functions are continuous and differentiable: this is not the case in the Cohesive Model, since the stresses are continuous and the displacements are discontinuous in the process zone.

Furthermore, during crack growth, the state of stress at the tip of the fictitious crack is known: at this point, in fact, the principal tensile stress equals the value of the material's ultimate tensile strength. The model makes it possible to describe size effect and ductile-to-brittle transition phenomena. The collapse brought about by the brittle propagation of the crack and described by Linear Elastic Fracture Mechanics (L.E.F.M.), is interpreted by the Cohesive Model as a *cusp catastrophe,* which is characterized by a softening branch with positive slope and referred to as *snap-back*.

3.4 Application of the cohesive model to masonry arches

3.4.1 The calculation algorithm

In this paragraph we will show the calculation reports, implemented in the MATLAB software to apply the cohesive model to the masonry arches.

To obtain the final algorithm, whose instructions are given in Paragraph 3.4.2, we started from an old calculation code, developed to analyze problems of beams simply supported and subjected to a simple bending moment, called FR.ANA (FRacture ANAlysis). This calculation code solves the problem of solving the system of n equations in 2 x n incoquite thanks to a mathematical artifact that uses an aux dimensional calculation matrix Aus(18x18) where 18 corresponds to the number of nodes in which the section is discretized. Therefore, by means of a numerical simulation to the finite elements, the Aus matrix has been adapted to a fictitious beam, which in addition to being subjected to a bending moment is also added to compression.

The implemented calculation algorithm, once defined the geometry of the arc to be studied, after having divided it into 16 parts (17 nodes), performs a linear elastic analysis and identifies the characteristics of the stresses (M, T and N) in the assigned nodes, due to the weight and the weight of the abutment. In the initial phase we consider a variable load q equal to zero. At this point, it identifies the most stressed node in terms of bending moment and applies the FR.ANA code with the modified Aus matrix to the section corresponding to this node. In this phase, the algorithm divides the section into 18 nodes and identifies the load necessary to create the crack, i.e. the load necessary for the fictitious crack tip to move from node i (edge) to node $i+1$. Following the displacement of the fictitious crack tip the algorithm estimates the new position of the real crack beam and performs a new elastic analysis of the structure. Phase two provides for the estimation of the Δq load necessary for the real fictitious tip to move to the next node. It is a process in control of crack opening. This is an iterative procedure where for each step you make:

1) calculation of the agents stresses in the section;

2) calculation of the load Δq necessary to move the fictitious crack tip to the next node;
3) check the position of the real crack tip;
4) recalculation of the position of the fictitious crack beam.

All this is repeated until the real crack tip reaches 90% of the height of the section.

It should be noted that, the algorithm implemented in addition to the cracking check carries out a check on the crusching section.

To model the true behavior of the material, a bilinear cohesive law was used for the process zone:

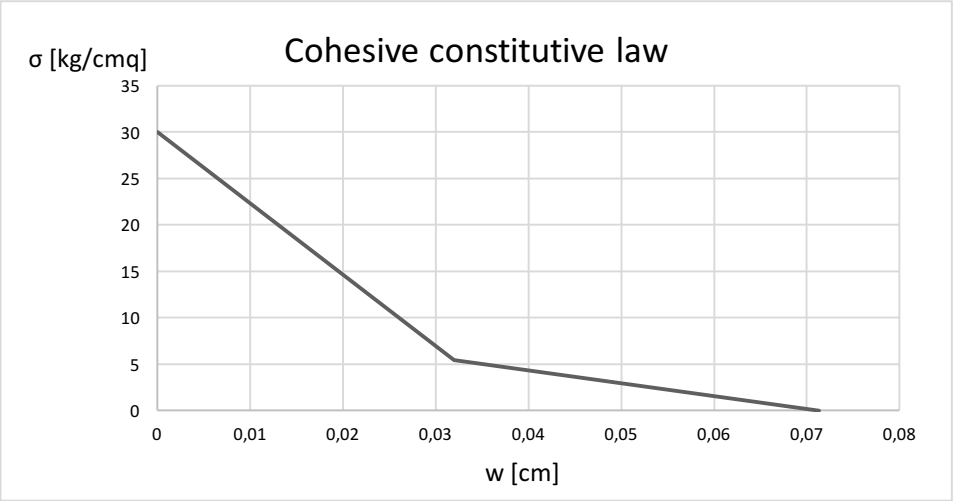

Chart 1 - Cohesive constitutive law used in the process zone.

Following are the main function of the calculation algorithm, implemented in Matlab, used:

- **Biutarc** (for more information to see Appendix 1). Represents the main program (mean). It governs the calls of the other "functions" of the

program and controls the progress of the processing flow. The operating scheme is as follows:

1) The general data of the problem are read. The arch is divided into 16 beam elements;
2) An elastic calculation is carried out in order to identify the section in which the crack will be born and propagate (called sez_cal);
3) The section identified in 18 nodes is subdivided;
4) The forces of reclosing, the openings and the displacement are calculated by effect of the own weight and of the variable load (initially equal to 0);
5) Based on the solution found in the previous step (4), the variable load is calculated so as to reach the tensile strength of the material in the fictitious tip (and then move this tip);
6) With this new variable load value the problem is solved again and it is verified if the real tip has to advance;
7) Starting from point 4.
8) Last phase sees the calculation of the variable load that produces the achievement of the ultimate compression tension of the material in the compressed limb.

- **Calcolo_P** (for more information to see Appendix 3). Once the section to be studied has been identified, this routin carries out the transition from the distributed load of the permanent loads to a concentrated load directed perpendicular to the axis of the part of the arch that will study it.

- **Fem** (for more information to see Appendix 5). It corresponds to the function that performs the linear analysis of the arch. It allows, in the first phase, to identify the sez_cal, i.e. the section in which the analysis will take place with the cohesive model. In the following steps it performs the elastic analyzes and estimate of the characteristics of the stresses in the section identified (sez_cal).
- **Legge_costitutiva** (for more information to see Appendix 6). This function starts from the cohesive law of the material used (see Chart 1) and transforms it into a matrix that allows the letcoe funcution to solve the problem:

$$cws = \begin{bmatrix} 0 & 30 & 0{,}04375 & 30 \\ 0{,}032 & 5{,}4 & 0{,}071 & 11 \\ 0{,}071 & 0 & 0{,}071 & 0 \end{bmatrix}$$

- **Letcoe** (for more information to see Appendix 7). This function reads the coefficients of influence from the cohesive array aus (18x18) and rewrites the vector coe(). This vector is used

  Once the vector coe() is obtained, the coefficients are passed, only those necessary to solve the system. Based on the opening of the slit in the previous step, establishes the f-w link of the nodes present in the cohesive tract through the csw() matrix, based on this modifies the coefficients of the matrix and the vector of the known terms in order to reduce the unknowns of the system.

  In practice in this function the Eq. (16) system is solved.

  For example:

DATA: matrix H, vector D, external force P (that of the previous step).
UNKNOWNS: vector w, vector F.

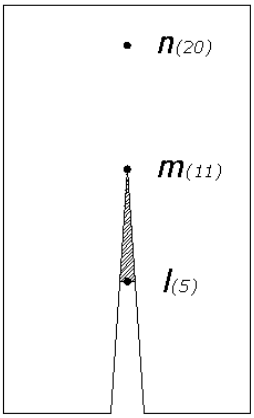

n ° equations: 20 - 5 + 1 = 16
unknowns w: 11 - 5 = 6
unknowns f: 20 - 5 + 1 = 16
Introducing however the constitutive law f-w of the cohesive tract (11 - 5) = 6 relations.
Therefore:
number of equations: 16
unknowns w: 0
unknown f: 16

- **Soluz** (for more information to see Appendix 9). This function calculates the slit openings w(), known as the forces of reclosing.

3.4.2 Matlab program instructions

The objective of the analysis carried out with the aid of MATLAB is the search for the maximum variable load (called "q") which leads to the formation of 4 brittle hinges (and therefore to a kinematism) along the development of the axis line of an arc of any geometry.

Several phases of initialization of the program are necessary (up to four phases, which is equivalent to the maximum number of hinge formation, but, if there is a symmetry of the arch, these can be reduced).

The program requires the following input data:

- Geometry of the arc axis line. You need to supply the x, y coordinates written in the vector form of the type:

$$\begin{cases} x = [x_1, x_2, \dots x_{17}] \\ y = [y_1, y_2, \dots y_{17}] \end{cases}$$

  and it is used as a unit of measure of the lengths cm;
- The modulus of linear elasticity "E" of the material constituting the arch in [kg/cm^2];
- The depth "b" and the height of the arch "h" in [cm] considered constant throughout the arc's development;
- Compression strength values "f_c" and traction "f_t" in [kg/cm^2];
- The weight per unit volume of "puv" abutments in [kg / cm^3];
- Height of the abutments from the "H" tax plane in [cm].

The arch axis line is divided into 16 beam elements (17 nodes) each of which is intended as a rectilinear structural element stuck at the ends (i and j) (to see Figure 23).

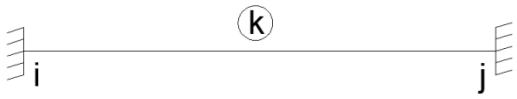

Figure 23 – Generic beam element.

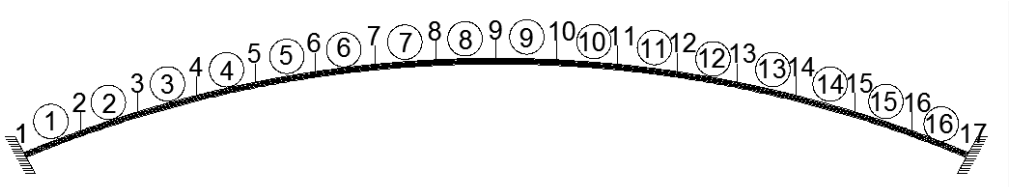

Figure 24 - Schematization of the arch.

Let M, T, N be the reactions to the joints and φ, v, w respectively the rotation and the two imposed displacements, assumed positive according to the convention shown in Figure 25, we have the following matrix relation:

$$\begin{bmatrix} M_i \\ T_i \\ N_i \\ M_j \\ T_j \\ N_j \end{bmatrix} = EI \begin{bmatrix} \frac{4}{\ell} & -\frac{6}{\ell^2} & 0 & \frac{2}{\ell} & \frac{6}{\ell^2} & 0 \\ -\frac{6}{\ell^2} & \frac{12}{\ell^3} & 0 & -\frac{6}{\ell^2} & -\frac{12}{\ell^3} & 0 \\ 0 & 0 & \frac{A}{I\ell} & 0 & 0 & -\frac{A}{I\ell} \\ \frac{2}{\ell} & -\frac{6}{\ell^2} & 0 & \frac{4}{\ell} & \frac{6}{\ell^2} & 0 \\ \frac{6}{\ell^2} & -\frac{12}{\ell^3} & 0 & \frac{6}{\ell^2} & \frac{12}{\ell^3} & 0 \\ 0 & 0 & -\frac{A}{I\ell} & 0 & 0 & \frac{A}{I\ell} \end{bmatrix} \begin{bmatrix} \varphi_i \\ v_i \\ w_i \\ \varphi_j \\ v_j \\ w_j \end{bmatrix} - \begin{bmatrix} M_i^0 \\ T_i^0 \\ N_i^0 \\ M_j^0 \\ T_j^0 \\ N_j^0 \end{bmatrix}.$$

This relation expresses the vector of the binding reactions as the sum of two contributions: the first deriving from the imposed displacements and the second from the equilibrium of the external loads acting on the beam.

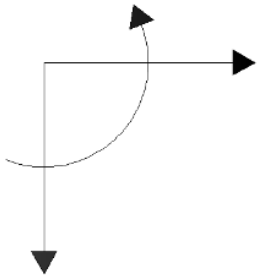

Figure 25 – Convetion of the sign.

The symmetric matrix (6x6) that multiplies the displacement vector is the stiffness matrix of the element and each column is obtained by imposing the

relative unit displacement or rotation and calculating the hyperstatic reactions at the extremes.

The second contribution is the vector of the forces equivalent to the external load, with the negative algebraic sign. In the case of uniformly distributed load "p", the carrier is:

$$Q = \left[-\frac{pl^2}{12}, \frac{pl}{2}, 0, \frac{pl^2}{12}, \frac{pl}{2}, 0\right]$$

Considering the "α" inclination of the structural element in question with respect to the uniformly distributed vertical load "p", we write:

$$Q = \left[-\frac{pl^2}{12}; \frac{pl\ cos\alpha}{2}; -\frac{pl\ sen\alpha}{2}; \frac{pl^2}{12}; \frac{pl\ cos\alpha}{2}; -\frac{pl\ sen\alpha}{2}\right]$$

The load "p" acting on each structural element is given by the sum of the own weights and the variable loads (structural unknown "q").
The weights are calculated by multiplying the weight per unit of volume of the arch abutments for the area of the same falling over the element multiplied by the depth and divided by the length of the element, or in formula:

$$p_{-proprio}(k) = \frac{puv * b * [(H - y_k) + (H - y_{k+1})]}{2} \quad (19)$$

From the first elastic analysis on the structure emerges the section that will be affected by the formation of the crack. Once this section has been identified, the program creates the conditions for applying the cohesive model, i.e. it calculates the component (P) perpendicular to the axis line of the element considered.

The program at each step calculates the value of the variable load such as to make the resulting P able to advance the fictitious crack tip.

The analysis stops in only two cases:

1. A slit depth of 90% of the height of the arc section in one of the 16 elements has been reached;
2. CRUSHING has been achieved in one of the 16 elements (overcoming the compressive strength).

The 1st PHASE OF INITIALIZATION is then started and the program is stopped. From the results we can see in which of the two cases we have reached and in which segment the crushing occurred or we reached an extension of the crack equal to 90% of the height of the section.

Once this part has been identified, in the subsequent phases we consider an elastic hinge, in the section analyzed in the previous phase, which indicates the impossibility of transmitting bending moment between the two adjacent sections.

Therefore in the subsequent phases, to structural elements that can be of 3 types and are indicated in Figure 26.

Figure 26 – 3 types of the structural elements used.

Taking into account the new structural elements (equipped with hinges) that compose the new axis line of the arch, a 2nd PHASE OF INITIALISATION is started (taking into account the presence of the last hinge formed in the previous phase, imposing that M = 0) which will lead to the formation of new hinges (due to CUSHING or the achievement of a 90% gap extension) in one or more new sections that will again be identified by starting the load from the value previously reached for the formation of the first hinge. This will be followed by a 3rd INITIALIZATION PHASE and a 4th INITIALIZATION PHASE in the case where asymmetric cases are analyzed for geometry or loads for which the formation of the hinges is not symmetrical along the whole arc development, until a kinematism is achieved (4 hinges) and then collapse.

What is derived from the program is precisely the value of the variable load that leads to the formation of new hinges.

4 Parametric analysis bases on the theoretical model

4.1 Descrizione of the application

In this chapter we will describe the results obtained by applying the cohesive crack model into false bridges in masonry arches. What unites these bridges are:

- The materials constituting the arch and abutment;
- The section of the arch;
- The length of the arch.

The arches analyzed have different degrees of lowering, that is, the relationship between arrow and length. Specifically, arches have been analyzed with a degree of lowering equal to 1/3, 1/4, 1/5, 1/6 and 1/7.

In the application of the program written in Matlab, referred to in the previous chapter, the cohesive model was applied to pre-defined masonry arches and we obtained the variable load value that we have the formation of a first pair of brittle hinges and the value with which we form the second pair of hinges. The arches analyzed are symmetric and symmetrically loaded.

Furthermore, for each arch, its behavior has been plotted, differentiating the "local" behavior found in the section in which the cracking and the "global" behavior of the structure during this phenomenon develops. In the first case, the variable load q, intended as a live load, was plotted, which is remembered having been modified according to the propagation of the crack, with the vertical displacement of the section in which the crack developed. While in the second one has studied what happened in terms of vertical displacement in the arch crown under the effect of the load q varied to accommodate the cracking conditions and because of the static changes induced by the progressive increase in the crack. This phase has been studied using the software to the finite elements SdC.

The fictitious cases analyzed are 5. In the first of the two following tables, some geometric data such as the arrow "f", the height "h" of the arch section, the width "b" of the examined bridge section and the maximum height "H" of the abutment are summarized on a case-by-case basis. In the second table summarizes some mechanical characteristics of the materials, such as the elasticity modulus "E", the weight per unit of volume "puv" of the material constituting the abutment, the compressive strength of the masonry "f_c" and tensile strength "f_t".

Case	**Degree of lowering**	**f** [cm]	**h** [cm]	**b** [cm]	**H** [cm]
1	1/3	1500	150	100	1710
2	1/4	1124	150	100	1335
3	1/5	900	150	100	1110
4	1/6	750	150	100	960

Case	Degree of lowering	f [cm]	h [cm]	b [cm]	H [cm]
5	1/7	642.8	150	100	853

Material	puv [kg/cm^3]	E [kg/cm^2]	fc [kg/cm^2]	ft [kg/cm^2]
Masonry	0.0025	300000	-500	30

4.2 Geometry with lowering 1/3

The first case examined concerns a bridge in masonry arch with a degree of lowering equal to 1/3. The geometrical characteristics are indicated in Figure 27.

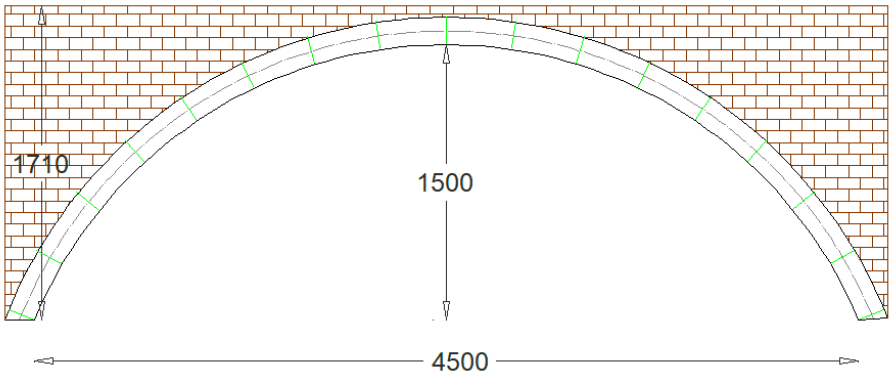

Figure 27 – Masonry arch with a degree of lowering equal to 1/3.

The cohesive crack model was applied to the geometries shown in Figure 27, using the program written in MATLAB, described in Chapter 3. The structure appears to be doubly interlocked, therefore we will look for the formation of n. 4 brittle hinges.

The fictitious bridge examined is symmetrical and, since we use a live load that is uniformly distributed, symmetrically loaded. Therefore, we will have the formation of pairs of contemporary hinges and to reach the desired number it was enough to use two initializations.

In the two different phases of initiation we obtained:

Phase	**n° of the hinges**	**Cause**	**n° node**	**q** [kg/cm]
1[a]	2	crushing	1 and 17	214.94
2[a]	2	crushing	3 and 15	77.71

In Figure 28 the results obtained are shown schematically the position of the brittle hinges.

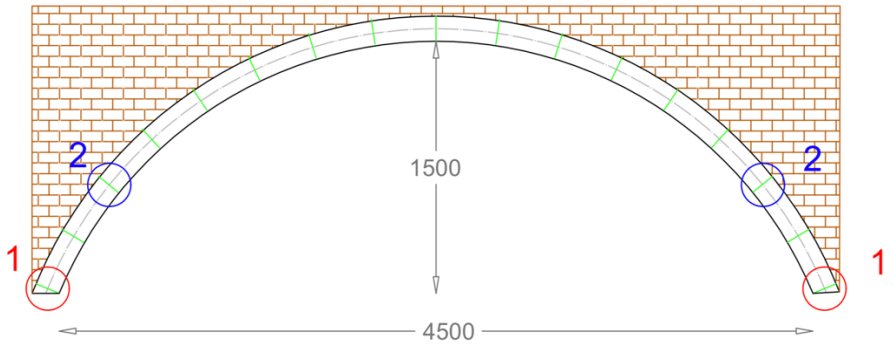

Figure 28 – Position of the brittle hinges in the arch.

Analyzing the results obtained, it is clear that once the first pair of hinges has been formed, in order to form the second one, a lower load is required, so that for the analyzed geometry the instantaneous formation of the four hinges can be obtained to the variable load of 214.94 kg/cm.

Another important aspect is that for the masonry arch with degree of lowering equal to 1/3 the cracking process is not obtained, i.e. the crushing is reached first.

4.3 Geometry with lowering 1/4

The Second case examined concerns a bridge in masonry arch with a degree of lowering equal to 1/4. The geometrical characteristics are indicated in Figure 29.

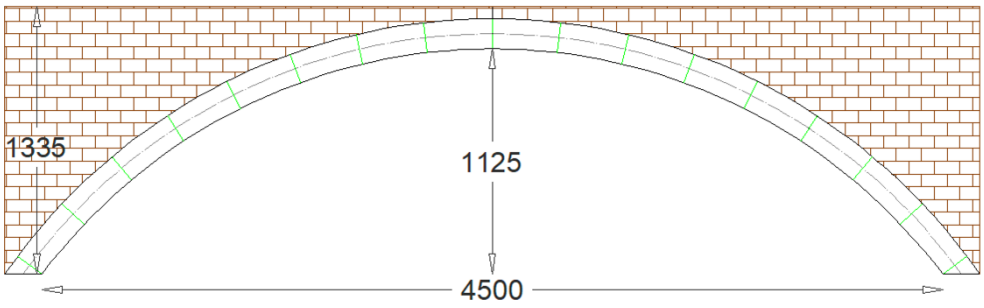

Figure 29 – Masonry arch with a degree of lowering equal to 1/4.

Also in this case, the structure appears to be doubly interlocked, therefore we will look for the formation of n. 4 brittle hinges.

The fictitious bridge examined is symmetrical and symmetrically loaded. Therefore we will have the formation of pairs of contemporary hinges and to reach the desired number it was enough to use two initializations.

In the two different phases of initiation we obtained:

Phase	n° of the hinges	Cause	n° node	q [kg/cm]
1ª	2	crushing	1 and 17	489.61
2ª	2	crushing	3 and 15	343.56

In Figure 30 the results obtained are shown schematically the position of the brittle hinges.

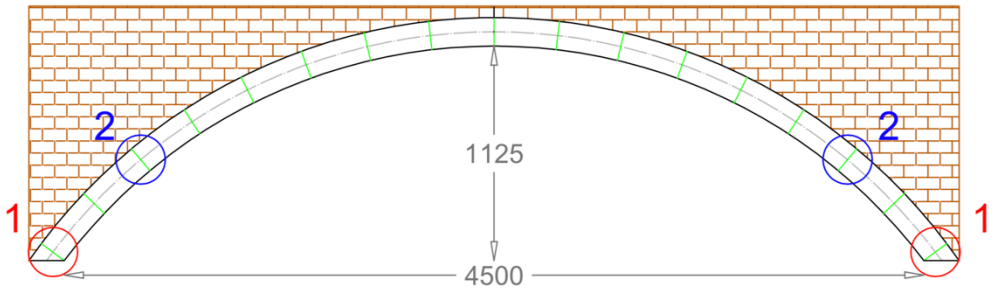

Figure 30 – Position of the brittle hinges in the arch.

Analyzing the results obtained, it is clear that once the first pair of hinges has been formed, in order to form the second one, a lower load is required, so that for the analyzed geometry the instantaneous formation of the four hinges can be obtained to the live load of 489.61 kg/cm.

If we want to compare the results obtained, it is clear that even for an arch with a degree of lowering equal to 1/4 the load necessary to initialize the cracking process is not reached. While the position of the brittle hinges in the two initialization phases remains the same.

4.4 Geometry with lowering 1/5

The third case examined concerns a bridge in masonry arch with a degree of lowering equal to 1/5. The geometrical characteristics are indicated in Figure 31.

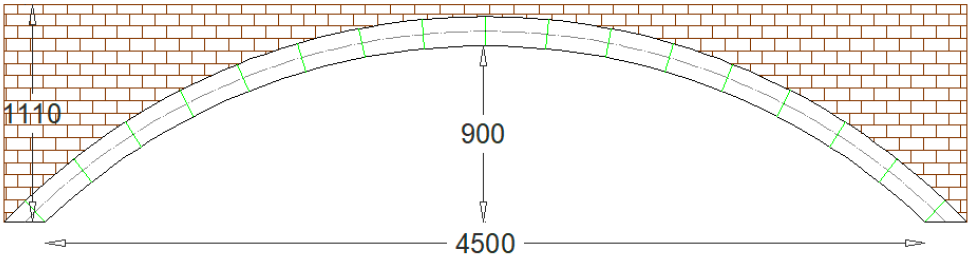

Figure 31 – Masonry arch with a degree of lowering equal to 1/5.

In this case the program shows a whole crack process. In fact, as can be seen from the results obtained shown in the following table, it is possible to obtain the formation of n. 4 brittle hinges for cracking.

Phase	n° of the hinges	Cause	n° node	q [kg/cm]
1[a]	2	cracking	1 and 17	353.78

Phase	n° of the hinges	Cause	n° node	q [kg/cm]
2[a]	2	cracking	3 and 15	444.20

In this case, during the first initialization phase the cohesive crack was advanced, which develops in node 1 and by symmetry in node 17.

Once the section in which the cracking process begins will be identified, the program divides this section into 18 nodes. The real crack tip and the fictitious crack tip will move on these nodes.

The following table shows the relevant results obtained from the iterations developed to conduct the crack (fictitious crack tip) up to 90% of the section height for the application of the cohesive crack model:

Step	ntipa	q [kN/m]	$\delta v_{(1\text{-}17)}$ [cm]	ξ [cm]
1	0	352	2	0,0
2	1	353.78	12	15.8
3	2	353.66	11.70	23.7
4	3	353.55	11.39	31.6
5	4	353.45	11.08	39.5
6	5	353.36	10.77	47.4
7	6	353.27	10.46	55.3
8	7	353.20	10.16	63.2
9	8	353.13	9.85	71.1
10	9	353.07	9.54	78.9
11	10	353.02	9.24	86.8
12	11	352.98	8.93	94.7
13	12	352.94	8.63	102.6
14	13	352.91	8.32	110.5
15	14	352.89	8.023	118.4
16	15	352.87	7.718	126.3

where:

ntipa: it is the position of the real crack tip ;

q: it is the live load;

δ_v: vertical displacement read at the section in which the crack takes place;

ξ: height of the crack

it is interesting to note how, once the load q has been obtained which causes the displacement of the real crack (step 2) towards the inside of the section, i.e. we have the birth of the real crack, the program, in the next step, identifies a lower load to advance the crack. This shows how the crack begins to open with the maximum load and continues to open monotonously as the load decreases in the softening phase.

In Chart 2 the vertical displacemente is plotted to vary of q.

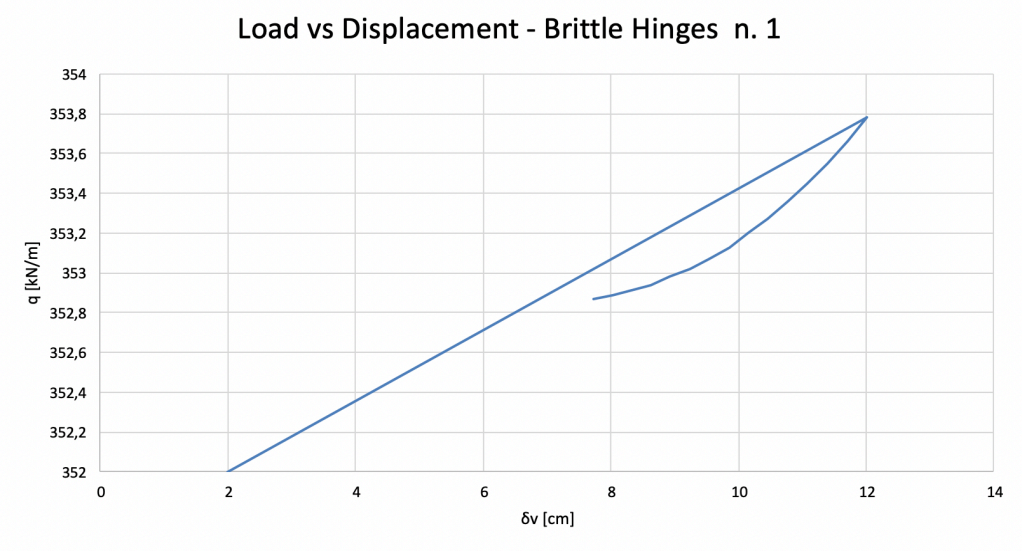

Chart 2 – Trend of the variable load vs displacement in control of advancement of the crack opening (w).

According to the Chart 2 we can see how, upon reaching the load q equal to 353.78 kg/cm, i.e. the load that produces the anazation of the real crack tip, and therefore the opening of the real crack tip, the behavior of the material in the softening phase shows a positive slope. In this case, once the maximum load is reached (q= 353.78 kg/cm) the load is vertically dropped. The softening trait is thus ignored and becomes virtual. In fact, to identify the softening section with positive slope it is necessary to pilot the loading process by opening the crack (w).

This is the typical behavior of relatively fragile materials (such as concrete, cast iron, glass, masonry, etc.), which have a low fracture energy value (G_{IC}).

The instability described above is called "snap-back". This instability represents a phenomenon included in the Catastrophe Theory.

Once the first phase of initialization has been completed, the program, once assigned a hinge in the cracked sections (1 and 17), resumes the anailisi and begins the second phase of initialization. In this phase, due to the geometry of the analyzed arch, the program identifies the birth of the cracking process in sections 3 and 15. The following table summarizes the results obtained from the application of the cohesive model:

Step	ntipa	q [kN/m]	$\delta v_{(3\text{-}15)}$ [cm]	ξ [cm]
1	0	442	3.50	0
2	1	444.20	12.02	15.8
3	2	444.04	11.72	23.7
4	3	443.89	11.41	31.6
5	4	443.76	11.1	39.5
6	5	443.63	10.79	47.4
7	6	443.52	10.48	55.3

Step	ntipa	q [kN/m]	$\delta v_{(3\text{-}15)}$ [cm]	ξ [cm]
8	7	443.42	10.17	63.2
9	8	443.34	9.87	71.1
10	9	443.26	9.56	78.9
11	10	443.20	9.25	86.8
12	11	443.14	8.95	94.7
13	12	443.09	8.64	102.6
14	13	443.05	8.34	110.5
15	14	443.02	8.03	118.4
16	15	443	7.73	126.3

Plotting the results of the application of the cohesive model, even in this case, a positive slope (phenomenon of the snap-back) is found for the "softening" section, as shown in Chart 3.

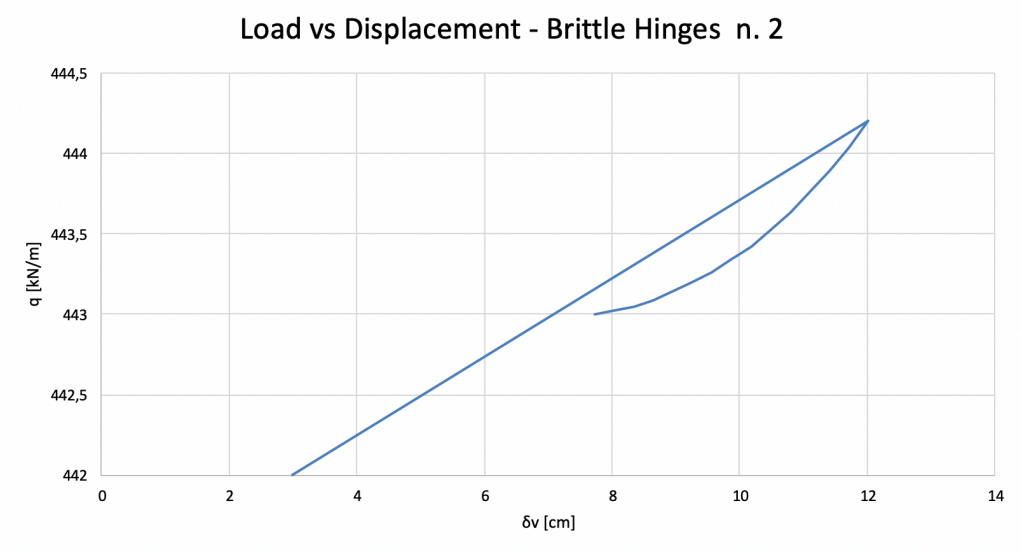

Chart 3 – Clear phenomenon of the snap-back in the second group of the brittle hinges in the arch with degree of lowering equal to 1/5.

Note the values of the variable load q, which is remembered to have been calculated in crack opening control (w), in a subsequent phase the overall structure of the arch was calculated for each iteration step of the initialization phase 1 and 2 vertical displacement, measured in the arch crown. To do this, the structure of the initial arch was created with finite elements. This model of the calculation was assigned the uniformly distributed load q, derived from the two previous phases. At each loading step:

1. For the first phase of initialization the moment of inertia of the section has been reduced in correspondence with the crack (section n. 1 and n. 17) to take into account, at each step, the progress of the real crack tip and therefore of the portion section no longer reagent;
2. For the second initialization phase a hinge was introduced in the completely cracked sections from the previous phase (section n. 1 and n. 17) and we proceeded as described in the previous point to take into account the progressive advancement of the crack (in the section n. 3 and n. 15).

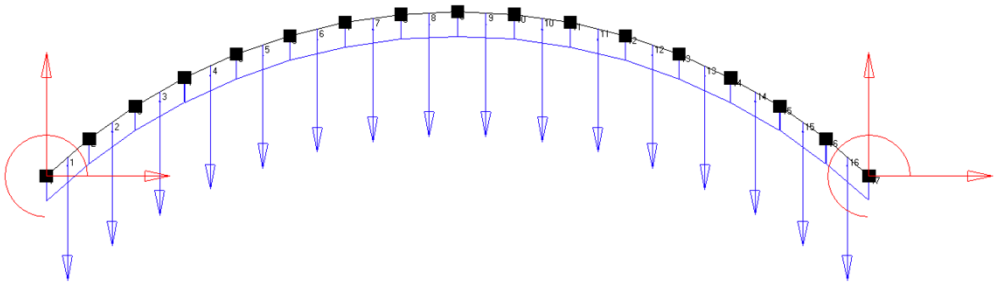

Figure 32 – FEM calculation scheme of arch with degree of lowering equal to 1/5.

For each loading phase, the vertical displacement in the arch crown was measured. The following table shows the results obtained:

q [kN/m]	δ [cm]
0	0.05558176
353.78	0.4717934
353.66	0.4917684
353.55	0.5125505
353.45	0.5341569
353.36	0.556732
353.27	0.580563
353.20	0.606723
353.13	0.6364917
353.07	0.6728707
353.02	0.7213555
352.98	0.7927232
352.94	0.9093977
352.91	1.121974
352.89	1.55454
352.87	2.524069
444.20	4.629277
444.04	4.632518
443.89	4.637092
443.76	4.643514
443.63	4.652184
443.52	4.664127
443.42	4.680449
443.34	4.70297
443.26	4.733971
443.20	4.777144
443.14	4.837199
443.09	4.921322
443.05	5.042167
443.02	5.234753
443.00	5.643672

Therefore, plotting the results obtained we find:

Chart 4 - Trend of the displacement of the arch crown to the variation of the live load q.

In Chart 4, points A, B and C are highlighted. These points represent:

A: starting point of the cracking process in sections 1 and 17;

B: points for reaching the maximum extension of the crack in sections 1 and 17 and formation of brittle hinges;

C: starting point of the cracking process in sections 3 and 15 due to the new loading process due to the change in the static scheme of the arch.

The structural behavior shown in Chart 4 is very interesting. in fact, looking at a focus of the chart, we notice an unstable trait that goes from A to B (to see Chart 5).

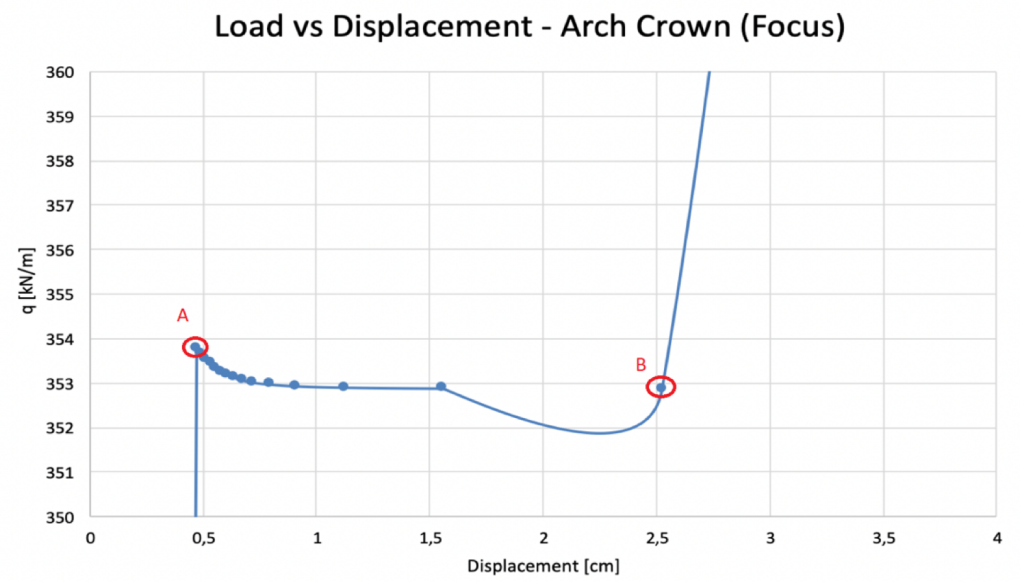

Chart 5 – Focus of the Chart 4.

Once point A is reached, to move forward and follow the crack process in sections 1 and 17 entirely, the load must decrease. Howeven, goes ahead even if the load decreases in sections 1 and 17, the fesseura advances, resulting in a progressive reduction in the stiffness of the sections themselves. This produces an increase in the vertical displacement in the arch crow and therefore a trait (A-B) which can be understood as a "structural softening" zone. Now, imagining to conduct the analysis in force control, as happens in reality, having reached point A, a small increase in load would lead directly to point B' suddenly (to see Chart 6), making the stroke A-B-B' a virtual stroke.

Ultimately, having arrived at the stationary point A, if we continue to increase the load q, it jumps discontinuously on the stable branch B'-P (to see Chart 6), which at a similar load shows a significantly greater lowering. From an energetic point of view, the energy returned by the system in jump A-B 'is equal to the

area subtended by the line AB', for the length of the arch. This energy will be transformed into the kinetic vibrational energy of the system around the condition represented by the point B'. The instability phenomenon just described, especially in the jump from A to B, is called snap-through.

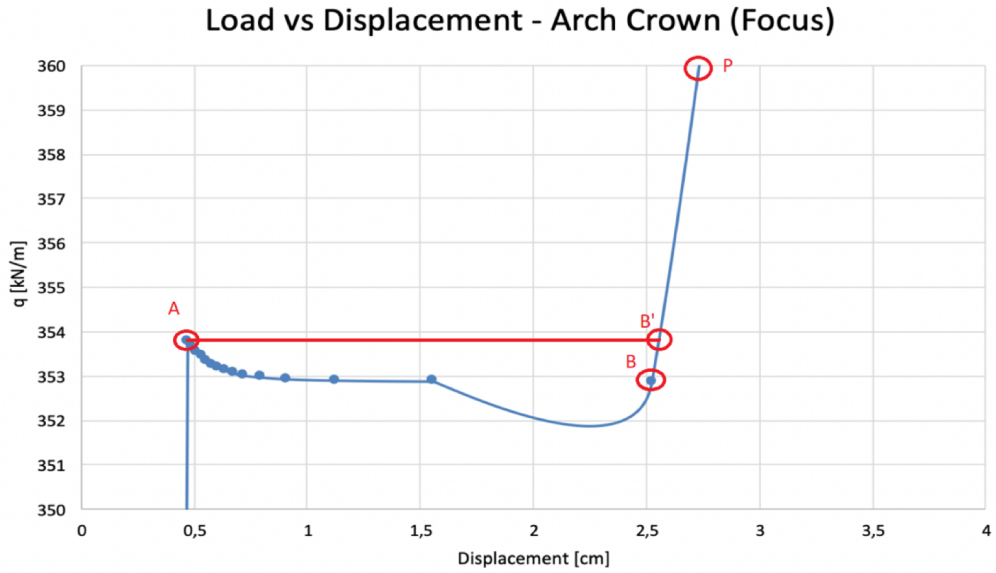

Chart 6 – Focus of the Chart 4 where the phenomenon of the snap-through is cleary shown

In conclusion, Figure 33 schematically shows the position of the n. 4 brittle hinges obtained.

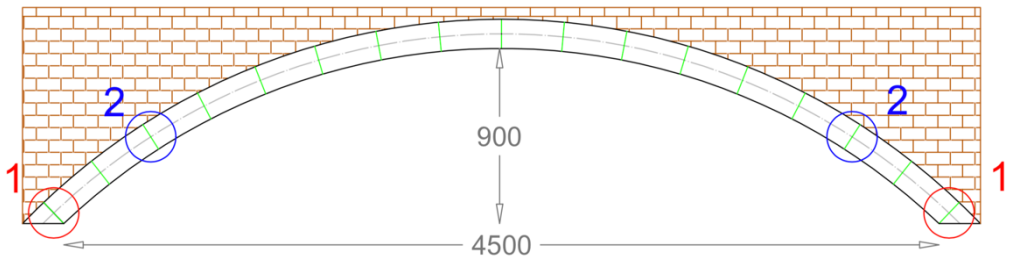

Figure 33 – Position of the brittle hinges in arch with degree of lowering equal to 1/5.

4.5 Geometry with lowering 1/6

The fourth case examined concerns a bridge in masonry arch with a degree of lowering equal to 1/6. The geometrical characteristics are indicated in Figure 34.

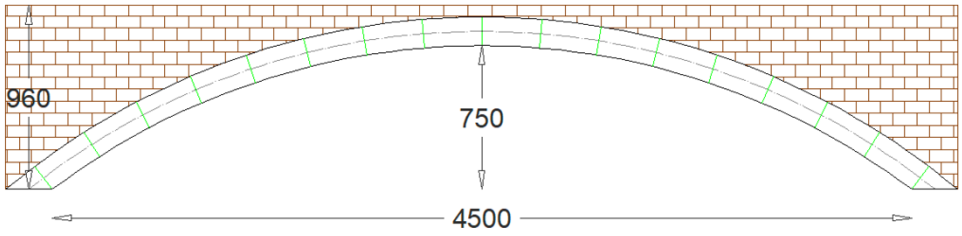

Figure 34 – Masonry arch with a degree of lowering equal to 1/6.

Also in this case the program shows a whole crack process. In fact, as can be seen from the results obtained shown in the following table, it is possible to obtain the formation of n. 4 brittle hinges for cracking.

Phase	n° of the hinges	Cause	n° node	q [kg/cm]
1ª	2	cracking	2 and 16	459.31
2ª	2	cracking	4 and 14	715.13

In this case, during the first initialization phase the cohesive crack was advanced, which develops in node 2 and by symmetry in node 16.

The following table shows the relevant results obtained from the iterations developed to conduct the crack (fictitious crack tip) up to 90% of the section height for the application of the cohesive crack model:

Step	ntipa	q [kN/m]	$\delta v_{(2\text{-}16)}$ [cm]	ξ [cm]
1	0	453.00	2.00	0.0
2	1	459.31	5.90	15.8
3	2	458.71	5.75	23.7
4	3	458.15	5.58	31.6
5	4	457.64	5.42	39.5
6	5	457.19	5.26	47.4
7	6	456.80	5.10	55.3
8	7	456.45	4.95	63.2
9	8	456.16	4.79	71.1
10	9	455.90	4.64	78.9
11	10	455.68	4.49	86.8
12	11	455.49	4.34	94.7
13	12	455.34	4.19	102.6
14	13	455.22	4.04	110.5
15	14	455.13	3.89	118.4
16	15	455.06	3.74	126.3

also in this case it is interesting to note how, once the load q has been obtained which causes the displacement of the real ctack (step 2) towards the inside of the section, i.e. we have the birth of the real crack, the program, in the next step, identifies a lower load to advance the crack. This shows how the crack begins to open with the maximum load and continues to open monotonously as the load decreases in the softening phase. It is clearly phenomenon of the snap-back (to see Chart 7).

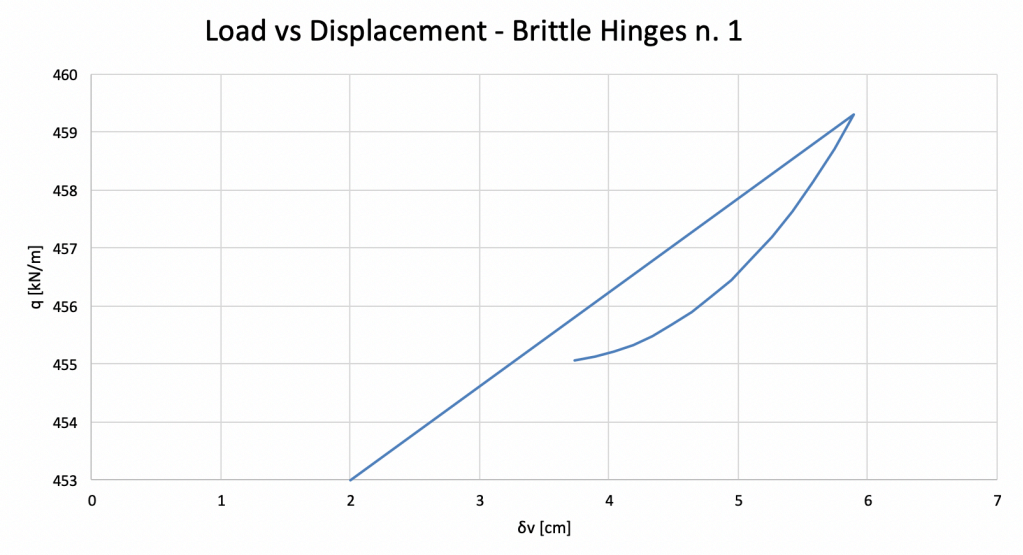

Chart 7 – Trend of the variable load vs displacement in control of advancement of the crack opening (w). Clear phenomenon of the snap-back in the first group of brittle hinges in arch with degree of lowering equal to 1/6

According to the Chart 7 we can see how, upon reaching the load q equal to 353.78 kg/cm, i.e. the load that produces the anazation of the real crack tip, and therefore the opening of the real crack tip, the behavior of the material in the softening phase shows a positive slope. In this case, once the maximum load is reached (q = 353.78 kg/cm) the load is vertically dropped. The softening trait is thus ignored and becomes virtual. In fact, to identify the softening section with positive slope it is necessary to pilot the loading process by opening the crack (w).

Once the first phase of initialization has been completed, the program, once assigned a hinge in the cracked sections (2 and 16), resumes the anailisi and begins the second phase of initialization. In this phase, due to the geometry of the analyzed arch, the program identifies the birth of the cracking process in

sections 4 and 14. The following table summarizes the results obtained from the application of the cohesive model:

Step	ntipa	q [kN/m]	$\delta v_{(4\text{-}14)}$ [cm]	ξ [cm]
1	0	715.00	10.00	0,0
2	1	715.80	46.85	15.8
3	2	715.72	45.67	23.7
4	3	715.64	44.40	31.6
5	4	715.57	43.30	39.5
6	5	715.50	42.11	47.4
7	6	715.44	40.93	55.3
8	7	715.38	39.74	63.2
9	8	715.34	38.56	71.1
10	9	715.29	37.37	78.9
11	10	715.25	36.19	86.8
12	11	715.22	35.00	94.7
13	12	715.19	33.82	102.6
14	13	715.17	32.63	110.5
15	14	715.14	31.44	118.4
16	15	715.13	30.25	126.3

Plotting the results of the application of the cohesive model, even in this case, a positive slope (phenomenon of the snap-back) is found for the "softening" section, as shown in Chart 8.

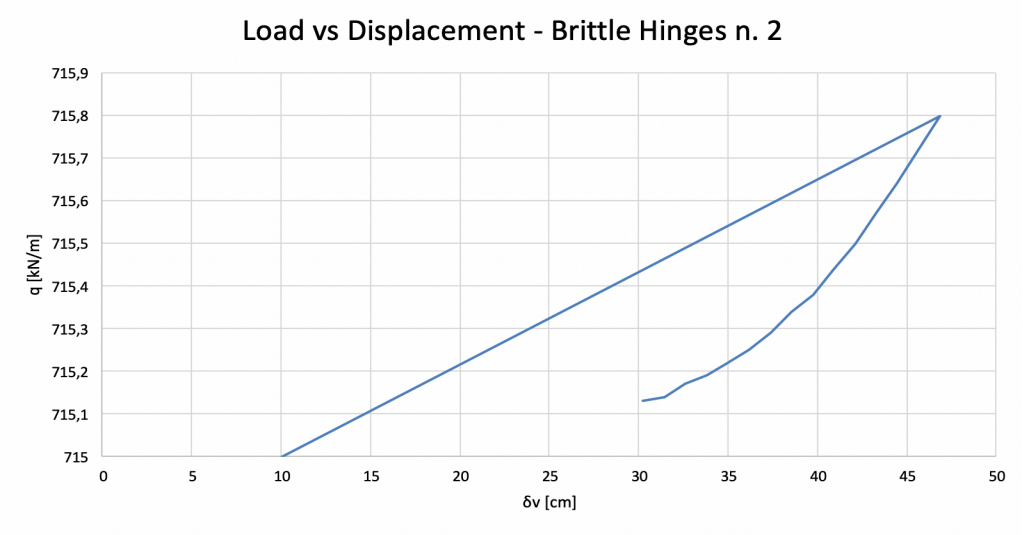

Chart 8 – Clear phenomenon of the snap-back in the second group of the brittle hinges in the arch with degree of lowering equal to 1/6.

Equally as done for arch with degree of lowering equal to 1/5, note the values of the variable load q, which is remembered to have been calculated in crack opening control (w), in a subsequent phase the overall structure of the arch was calculated for each iteration step of the initialization phase 1 and 2 vertical displacement, measured in the arch crown with the finite elements. This model of calculation was assigned the uniformly distributed load q, derived from the two previous phases:

1. For the first phase of initialization the moment of inertia of the section has been reduced in correspondence with the crack (section n. 2 and n. 16) to take into account, at each step, the progress of the real crack tip and therefore of the portion section no longer reagent;
2. For the second initialization phase a hinge was introduced in the completely cracked sections from the previous phase (section n. 2 and

n. 16) and we proceeded as described in the previous point to take into account the progressive advancement of the crack (in the section n. 4 and n. 14).

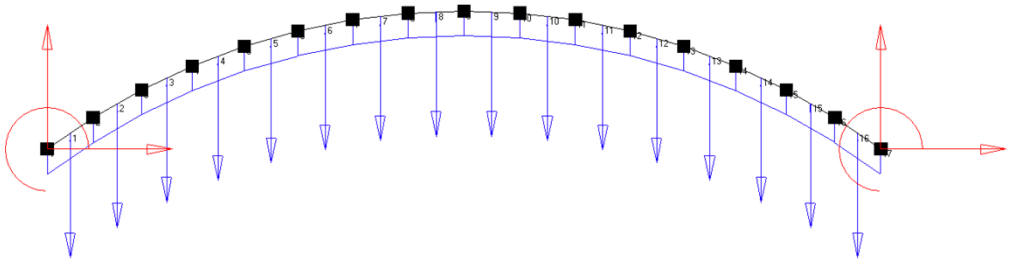

Figure 35 – FEM calculation scheme of arch with degree of lowering equal to 1/6.

For each loading phase, the vertical displacement in the arch crown was measured. The following table shows the results obtained:

q [kN/m]	δ [cm]
0	0.03590795
459.31	0.3483266
458.71	0.3496106
458.15	0.3513696
457.64	0.353774
457.19	0.3570736
456.80	0.36136398
456.45	0.3680452
456.16	0.3772681
455.90	0.3909369
455.68	0.4120263
455.49	0.4461711
455.34	0.5048064
455.22	0.6126329
455.13	0.8257242
455.06	1.265398

q [kN/m]	δ [cm]
715.80	1.887031
715.72	1.887565
715.64	1.8883
715.57	1.889331
715.50	1.890738
715.44	1.892705
715.38	1.895445
715.34	1.899388
715.29	1.905084
715.25	1.913655
715.22	1.927107
715.19	1.949538
715.17	1.990807
715.14	2.079163
715.13	2.3196

Therefore, plotting the results obtained we find:

Chart 9 - Trend of the displacement of the arch crown to the variation of the live load q.

In Chart 4, points A, B and C are highlighted. These points represent:

A: starting point of the cracking process in sections 2 and 16;

B: points for reaching the maximum extension of the crack in sections 2 and 16 and formation of brittle hinges;

C: starting point of the cracking process in sections 4 and 14 due to the new loading process due to the change in the static scheme of the arch.

In this case, looking at the Chart 9, the snap-through phenomenon is clearly visible. However, looking at a focus of the Chart 10 the "jump" linked to the instability is clearer:

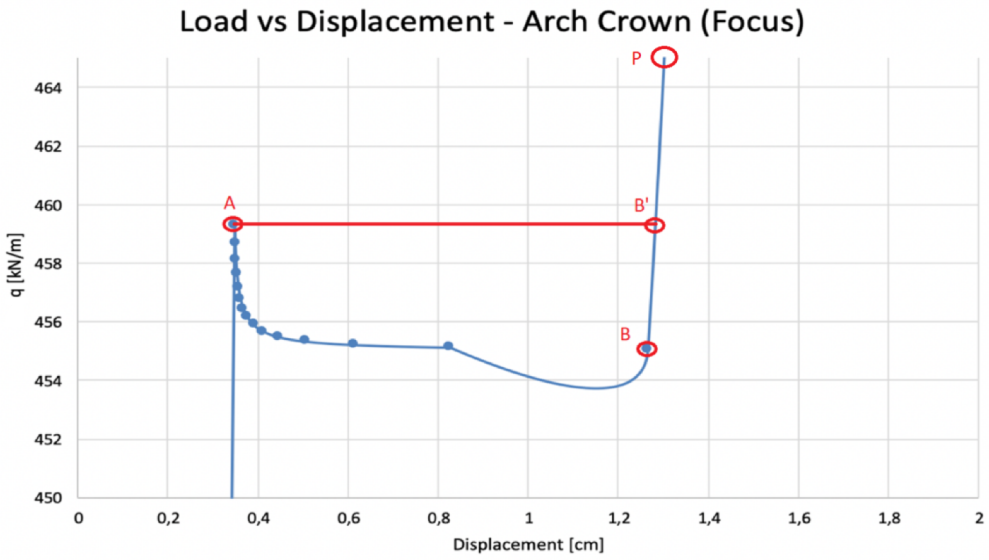

Chart 10 – Focus of the Chart 9 where the phenomenon of the snap-through is clearly visible.

In the same way as the case seen in the previous paragraph, we notice the phenomenon of the snap-through. In fact, having arrived at the stationary point A, if we continue to increase the load q, it jumps discontinuously on the stable branch B'-P (to see Chart 10), which at a similar load shows a significantly greater lowering. From an energetic point of view, the energy returned by the system in jump A-B 'is equal to the area subtended by the line AB', for the length of the arch. This energy will be transformed into the kinetic vibrational energy of the system around the condition represented by the point B'.

In conclusion, Figure 36 schematically shows the position of the n. 4 brittle hinges obtained.

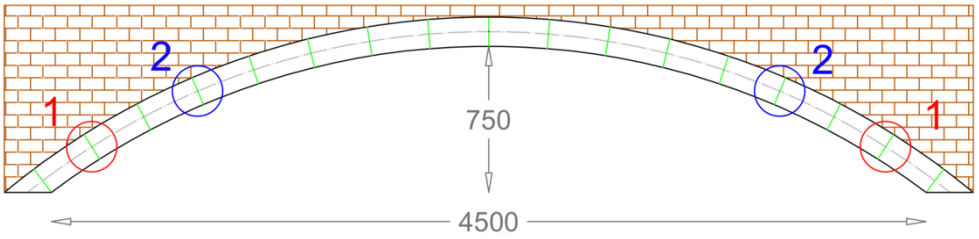

Figure 36 – Position of the brittle hinges in arch with degree of the lowering equal to 1/6.

4.6 Geometry with lowering 1/7

The last case examined concerns a bridge in masonry arch with a degree of lowering equal to 1/7. The geometrical characteristics are indicated in Figure 37.

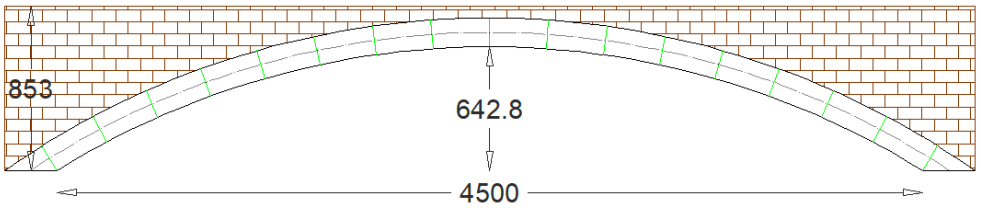

Figure 37 – Masonry arch with a degree of lowering equal to 1/7.

Also in this case, the program shows a whole crack process. In fact, as can be seen from the results obtained shown in the following table, it is possible to obtain the formation of n. 4 brittle hinges for cracking.

Phase	n° of the hinges	Cause	n° node	q [kg/cm]
1ª	2	cracking	2 and 16	408.62
2ª	2	cracking	5 and 13	690.28

In this case, during the first initialization phase the cohesive crack was advanced, which develops in node 2 and by symmetry in node 16.

The following table shows the relevant results obtained from the iterations developed to conduct the crack (fictitious crack tip) up to 90% of the section height for the application of the cohesive crack model:

Step	ntipa	q [kN/m]	$\delta v_{(2\text{-}16)}$ [cm]	ξ [cm]
1	0	404.00	2.30	0.0
2	1	408.62	6.02	15.8
3	2	408.07	5.87	23.7

4	3	407.55	5.71	31.6
5	4	407.09	5.54	39.5
6	5	406.68	5.37	47.4
7	6	406.31	5.21	55.3
8	7	405.99	5.05	63.2
9	8	405.72	4.89	71.1
10	9	405.48	4.74	78.9
11	10	405.28	4.58	86.8
12	11	405.11	4.43	94.7
13	12	404.97	4.27	102.6
14	13	404.86	4.12	110.5
15	14	404.78	3.97	118.4
16	15	404.72	3.82	126.3

also in this case it is interesting to note how, once the load q has been obtained which causes the displacement of the real crack (step 2) towards the inside of the section, i.e. we have the birth of the real crack, the program, in the next step, identifies a lower load to advance the crack. This shows how the crack begins to open with the maximum load and continues to open monotonously as the load decreases in the softening phase. It is clearly phenomenon of the snap-back (to see Chart 11)

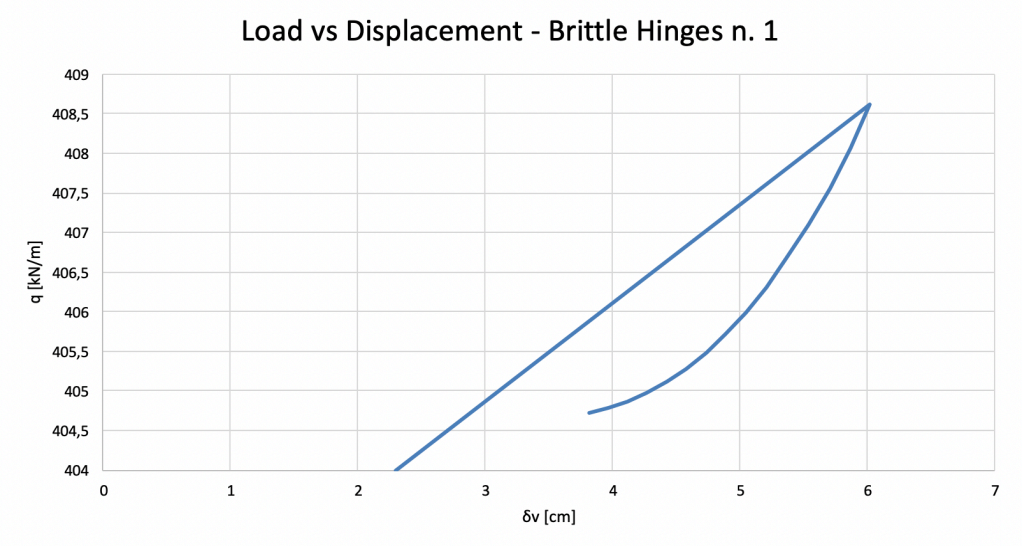

Chart 11 – Trend of the variable load vs displacement in control of advancement of the crack opening (w). Clear phenomenon of the snap-back in the first group of brittle hinges in arch with degree of lowering equal to 1/7

According to the Chart 11 we can see how, upon reaching the load q equal to 408.62 kg/cm, i.e. the load that produces the anazation of the real crack tip, and therefore the opening of the real crack tip, the behavior of the material in the softening phase shows a positive slope. In this case, once the maximum load is reached (q= 408.62 kg/cm) the load is vertically dropped. The softening trait is thus ignored and becomes virtual. In fact, to identify the softening section with positive slope it is necessary to pilot the loading process by opening the crack (w).

Once the first phase of initialization has been completed, the program, once assigned a hinge in the cracked sections (2 and 16), resumes the anailisi and begins the second phase of initialization. In this phase, due to the geometry of the analyzed arch, the program identifies the birth of the cracking process in sections 5 and 13. This last result is very interesting. In fact, remembering that

the second initialization phase led to the formation of the second pair of hinges in the sections:

- 3-15 for arch with degree of lowering 1/5;
- 4-14 for arch with degree of lowering 1/6;
- 5-13 for arch with degree of lowering 1/7;

it is clear how, as the degree of lowering decreases, the position of the second pair of hinges moves towards the arch crown of the arch. This highlights how, if the degree of lowering decreases, we have a transition from the arch behavior to the beam behavior.

The following table summarizes the results obtained from the application of the cohesive model:

Step	ntipa	q [kN/m]	$\delta v_{(5\text{-}13)}$ [cm]	ξ [cm]
1	0	689.00	10.00	0.0
2	1	690.28	45.65	15.8
3	2	690,20	44.50	23.7
4	3	690.11	43.35	31.6
5	4	690.04	42.19	39.5
6	5	689.97	41.03	47.4
7	6	689.91	39.88	55.3
8	7	689.85	38.72	63.2
9	8	689.80	37.57	71.1
10	9	689.76	36.42	78.9
11	10	689.72	35.26	86.8
12	11	689.68	34.10	94.7
13	12	689.65	32.94	102.6
14	13	689.63	31.79	110.5
15	14	689.61	30.63	118.4
16	15	689.59	29.47	126.3

Plotting the results of the application of the cohesive model, even in this case, a positive slope (phenomenon of the snap-back) is found for the "softening" section, as shown in Chart 12.

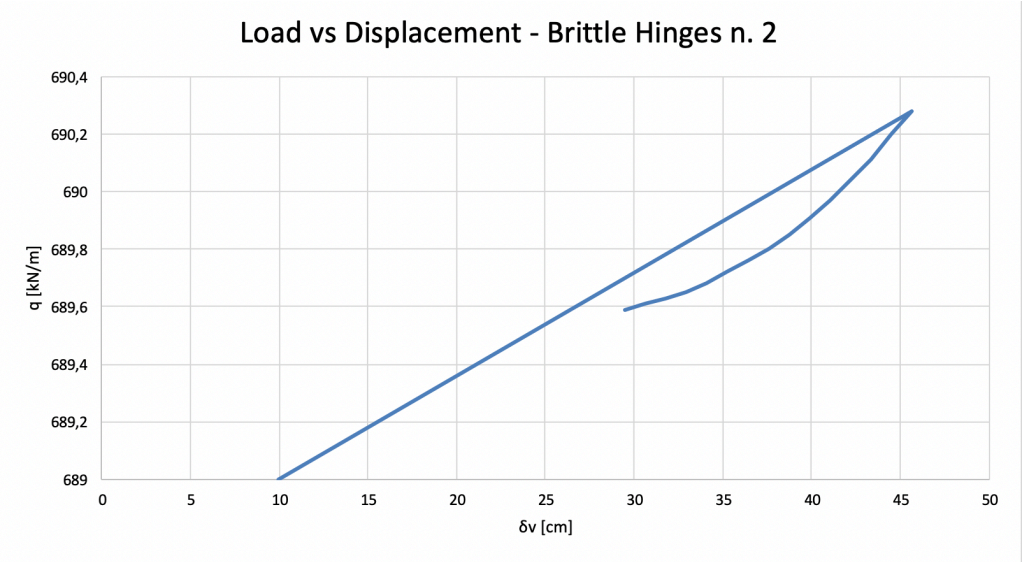

Chart 12 – Clear phenomenon of the snap-back in the second group of the brittle hinges in the arch with degree of lowering equal to 1/7.

Equally as done for arches with degree of lowering equal to 1/5 and to 1/6, note the values of the variable load q, which is remembered to have been calculated in crack opening control (w), in a subsequent phase the overall structure of the arch was calculated for each iteration step of the initialization phase 1 and 2 vertical displacement, measured in the arch crown with the finite elements. This model of the calculation was assigned the uniformly distributed load q, derived from the two previous phases:

1. For the first phase of initialization the moment of inertia of the section has been reduced in correspondence with the crack (section n. 2 and n.

16) to take into account, at each step, the progress of the real crack tip and therefore of the portion section no longer reagent;

2. For the second initialization phase a hinge was introduced in the completely cracked sections from the previous phase (section n. 2 and n. 16) and we proceeded as described in the previous point to take into account the progressive advancement of the crack (in the section n. 5 and n. 13).

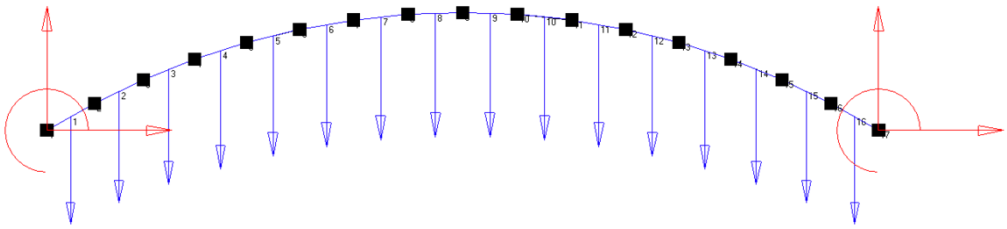

Figure 38 – FEM calculation scheme of arch with degree of lowering equal to 1/7.

For each loading phase, the vertical displacement in the arch crown was measured. The following table shows the results obtained:

q [kN/m]	δ [cm]
0.00	0.02435273
408.62	0.2081952
408.07	0.2089852
407.55	0.2100604
407.09	0.2135436
406.68	0.2163117
406.31	0.2201945
405.99	0.225772
405.72	0.2340284
405.48	0.2467577
405.28	0.2511272

q [kN/m]	δ [cm]
405.11	0.2673622
404.97	0.3027611
404.86	0.3679492
404.78	0.4972966
404.72	0.7670499
690.28	0.9333968
690.20	0.935886
690.11	0.9390113
690.04	0.9430132
689.97	0.9481436
689.91	0.9459039
689.85	0.9541984
689.80	0.9651587
689.76	0.9797988
689.72	0.9996402
689.68	1.02728
689.65	1.067996
689.63	1.134858
689.61	1.267287
689.59	1.614586

Therefore, plotting the results obtained we find:

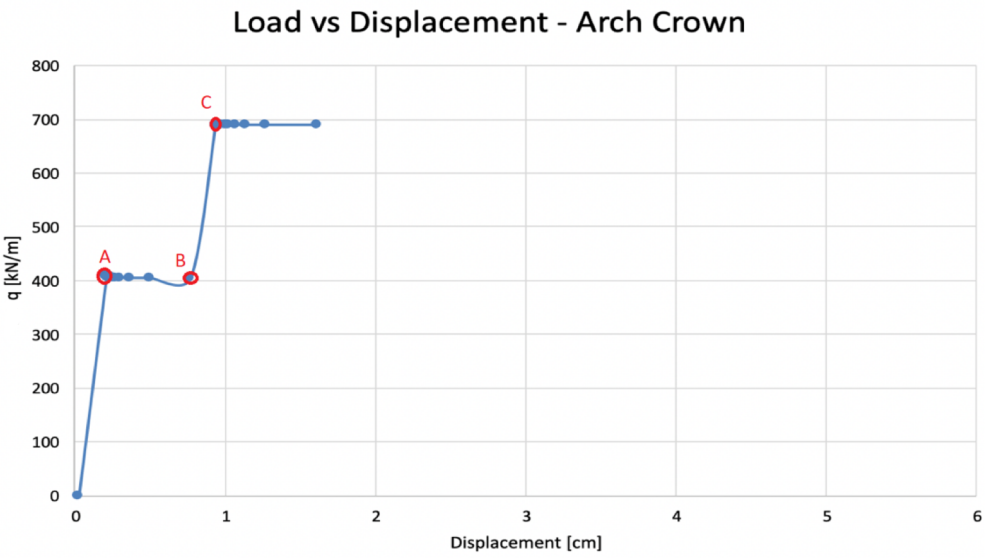

Chart 13 - Trend of the displacement of the arch crown to the variation of the live load q.

In Chart 13, points A, B and C are highlighted. These points represent:

A: starting point of the cracking process in sections 2 and 16;

B: points for reaching the maximum extension of the crack in sections 2 and 16 and formation of brittle hinges;

C: starting point of the cracking process in sections 5 and 13 due to the new loading process due to the change in the static scheme of the arch.

In this case, looking at the Chart 13, the snap-through phenomenon is clearly visible. However, looking at a focus of the Chart 14 the "jump" linked to the instability is clearer:

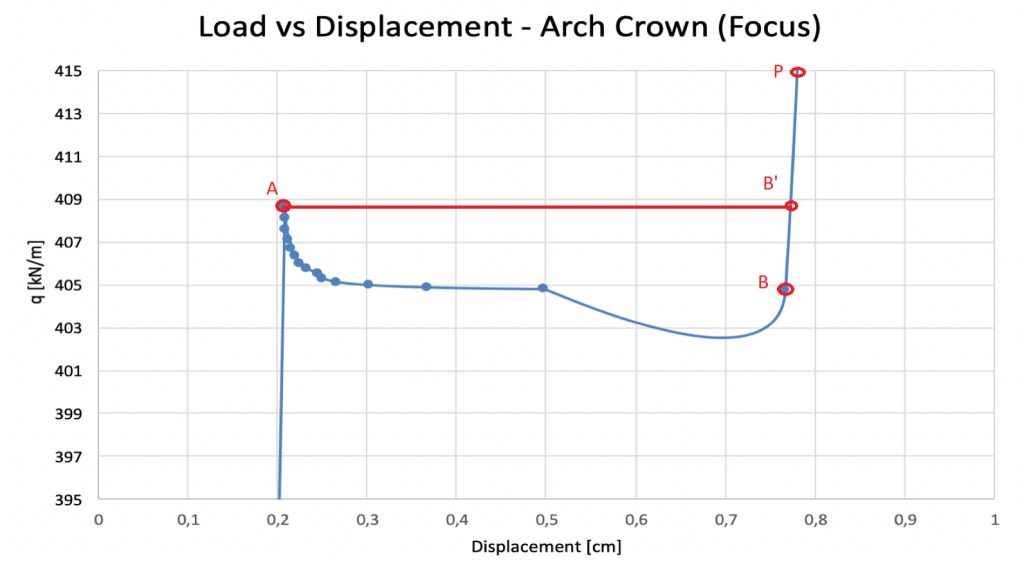

Chart 14 – Focus of the Chart 13 where the phenomenon of the snap-through is clearly visible.

In the same way as the case seen in the previous paragraph, we notice the phenomenon of the snap-through. In fact, having arrived at the stationary point A, if we continue to increase the load q, it jumps discontinuously on the stable branch B'-P (to see Chart 14), which at a similar load shows a significantly greater lowering. From an energetic point of view, the energy returned by the system in jump A-B 'is equal to the area subtended by the line AB', for the length of the arch. This energy will be transformed into the kinetic vibrational energy of the system around the condition represented by the point B'.

In conclusion, Figure 39 schematically shows the position of the nos. 4 brittle hinges obtained.

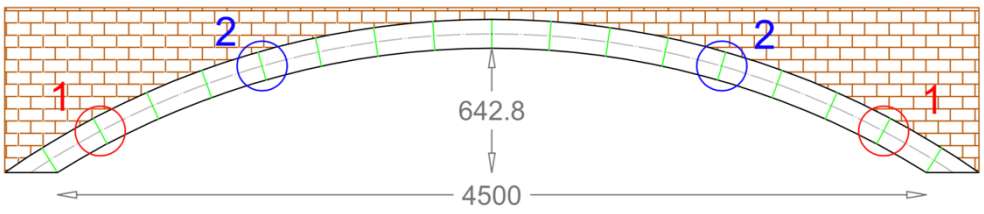

Figure 39 – Position of the brittle hinges in arch with degree of the lowering equal to 1/6.

5 The case study: Mosca Bridge

5.1 Historical view of Mosca Bridge

The Moscow Bridge is the most audacious construction carried out in Turin in the first half of the 1800s, it takes its name from the author, Carlo Bernardo Mosca, who had to fight against the distrust and meanness of many "experts" in order to realize his masterpiece. the consequent opposition of the municipal administration to a project considered even reckless (the same struggle that, forty years later, will have to support Alessandro Antonelli to make accept the bold construction of the Mole). In Figure 40 there is an illustration of the Bridge located on the Dora River, in correspondence of Corso Giulio Cesare.

The bridge designs presented by French engineers in 1812 included three or even five arched structures. When Moscow, ten years later, was commissioned to study the same problem, he proposed a more daring solution, devising a single-span bridge, of great light and strongly lowered. Moscow illustrated his project in which he proposed "... the maximum accuracy and precision, both in the apparatus in the cutting stones, as in the most minute construction warnings ...".

Figure 40 – Mosca Bridge over the Dora River in Turin (Italy)

(image by authors).

The Moscow Bridge was built between 1823 and 1828, this bridge achieved European fame both for the audacity of the project and for the perfection of the execution. Unfortunately, today the majority ignore its existence, but once the inhabitants of Turin were proud of it, and in addition to their sober elegance, they admired their exceptional slenderness, so difficult to obtain with the stone structure.

The structural typology and the execution technique make this work classify as a Perronet type bridge. The artifice designed to obtain the real arch faithful to the design was to build the rib raised above the project profile. At the time of disarming, the relative displacement of the segments, resulting from the deformation due to their own weight and expected almost exactly by the author, brought the side surfaces of the blocks into contact. The method, already tested by some builders on bridges of lesser light, was applied by

Moscow with particular precautions and the result obtained was exceptional. The ashlars were brought into contact so as to form a monolithic structure and the shape of the arch approached that designed in such a measure that the lowering (ratio between the arrow of the arch and the rope) in the real bridge is 0.123 while on the drawing it was 0.122.

Figure 41 - Original structural model of the Mosca Bridge (19th century), Dept. of Structural, Geotechnical and Building Engineering, Politecnico di Torino (Italy) (image by authors).

The total length of the bridge, including the entrance yards, is 129 meters and the width is 13.7 meters. The structure entirely in cut stone is a single, strongly lowered arch; the intrados is an arc of a circle of 5.5 meters of arrow and 45 meters of rope. The cylindrical vault, constructed from 93 courses of ashlars, has a key thickness of 1.5 meters. The material used for the structure is exclusively Malanaggio stone, a gneiss with mechanical characteristics similar to those of granite, of a pleasant greenish gray color that is maintained over time. The entire requirement was extracted from the main quarry of the Malanaggio, near Pinerolo.

5.2 Application of the cohesive crack model to Mosca Bridge

The geometric and mechanical data relating to the Mosca Bridge, in order to perform the calculation, are represented in Figure 42 and summarized in the following table, whose meaning has already been explained in Chapter 3:

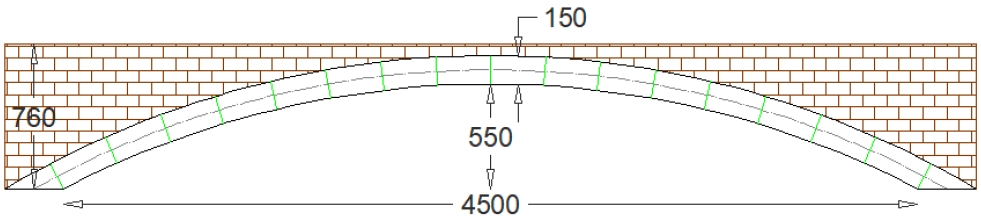

Figure 42 – Geometric of the Mosca Bridge.

Material	**b** [cm]	**h** [cm]	**puv** [kg/cm^3]	**E** [kg/cm^2]	**fc** [kg/cm^2]	**ft** [kg/cm^2]
Masonry	100	150	0.0025	300000	-500	30

The weight per volume unit, equal to 0.0025 kg/cm^3, was calculated as the average between the weight per unit volume of the Manalaggio stone (equal to 0.0027 kg/cm^3) which constitutes the arc and the weight of the filling (equal to 0.0023 kg/cm^3).

The following table summarizes the results obtained from the two initialization phases:

Phase	**n° of the hinges**	**Cause**	**n° node**	**q** [kg/cm]
1^a	2	cracking	2 and 16	364.59

Phase	n° of the hinges	Cause	n° node	q [kg/cm]
2[a]	3	cracking	8, 9 and 10	465,80

In this case, during the first initialization phase the cohesive crack was advanced, which develops in node 2 and by symmetry in node 16.

The following table shows the relevant results obtained from the iterations developed to conduct the crack (fictitious crack tip) up to 90% of the section height for the application of the cohesive crack model:

Step	ntipa	q [kN/m]	$\delta v_{(2\text{-}16)}$ [cm]	ξ [cm]
1	0	0.00	0.00	0.0
2	1	364,59	5.95	15.8
3	2	364,03	5.80	23.7
4	3	363,50	5.63	31.6
5	4	363,03	5.47	39.5
6	5	362,61	5.31	47.4
7	6	362,23	5.14	55.3
8	7	361,91	4.98	63.2
9	8	361,63	4.83	71.1
10	9	361,39	4.67	78.9
11	10	361,19	4.52	86.8
12	11	361,02	4.36	94.7
13	12	360,88	4.21	102.6
14	13	360,77	4.06	110.5
15	14	360,68	3.91	118.4
16	15	360,62	3.76	126.3

where:

ntipa: it is the position of the real crack tip;

q: it is the variable load;

δ_v: vertical displacement read at the section in which the crack takes place;

ξ: height of the crack

also in this case it is interesting to note how, once the load q has been obtained which causes the displacement of the real crack (step 2) towards the inside of the section, i.e. we have the birth of the real crack, the program, in the next step, identifies a lower load to advance the crak. This shows how the crack begins to open with the maximum load and continues to open monotonously as the load decreases in the softening phase. It is clearly phenomenon of the snap-back (to see Chart 15).

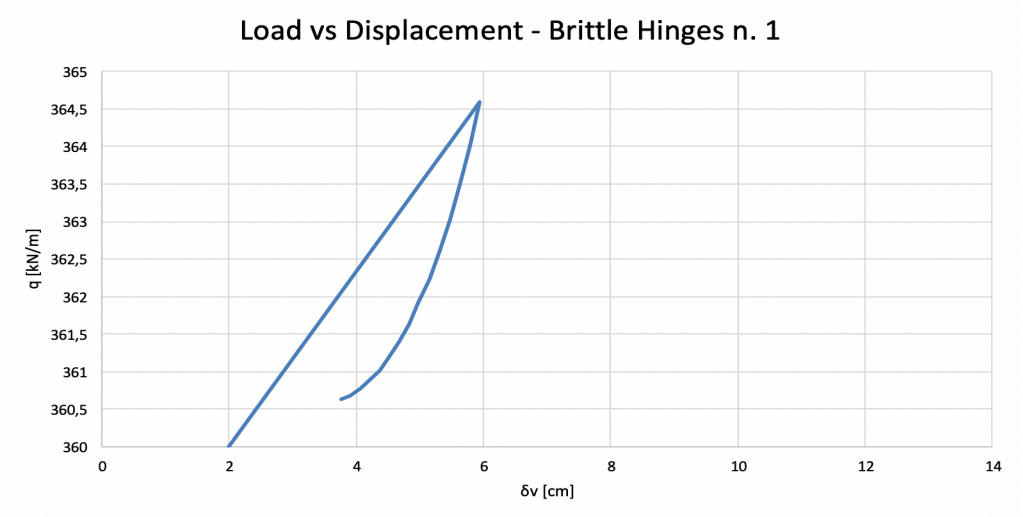

Chart 15 – Trend of the variable load vs displacement in control of advancement of the crack opening (w). Clear phenomenon of the snap-back in the first group of brittle hinges in Mosca Bridge

According to the Chart 15 we can see how, upon reaching the load q equal to 364,59 kg/cm, i.e. the load that produces the anazation of the real crack tip, and therefore the opening of the real crack tip, the behavior of the material in the softening phase shows a positive slope. In this case, once the maximum

load is reached (q= 364,59 kg/cm) the load is vertically dropped. The softening trait is thus ignored and becomes virtual. In fact, to identify the softening section with positive slope it is necessary to pilot the loading process by opening the crack (w).

Once the first phase of initialization has been completed, the program, once assigned a hinge in the cracked sections (2 and 16), resumes the anailisi and begins the second phase of initialization. In this phase, due to the geometry of the analyzed arch, the program identifies the birth of the cracking process in sections 8,10 and in addition, a crack is born in the section n. 9. According to the paragraph, the results obtained show how an increase in the degree of lowering leads to the formation of hinges in the sections next to the arch crown.

The following table summarizes the results obtained from the application of the cohesive model:

Step	**ntipa**	**q [kN/m]**	**$\delta v_{(8\text{-}9\text{-}10)}$ [cm]**	**ξ [cm]**
1	0	0.00	7.00	0.0
2	1	465.80	38.82	15.8
3	2	465.72	37.84	23.7
4	3	465.64	36.86	31.6
5	4	465.57	35.87	39.5
6	5	465.50	34.89	47.4
7	6	465.44	33.91	55.3
8	7	465.39	32.93	63.2
9	8	465.34	31.94	71.1
10	9	465.30	30.96	78.9
11	10	465.26	29.97	86.8
12	11	465.23	28.99	94.7
13	12	465.20	28.01	102.6
14	13	465.18	27.02	110.5
15	14	465.16	26.04	118.4

Step	ntipa	q [kN/m]	$\delta v_{(8\text{-}9\text{-}10)}$ [cm]	ξ [cm]
16	15	465.14	25.05	126.3

Plotting the results of the application of the cohesive model, even in this case, a positive slope (phenomenon of the snap-back) is found for the "softening" section, as shown in Chart 16.

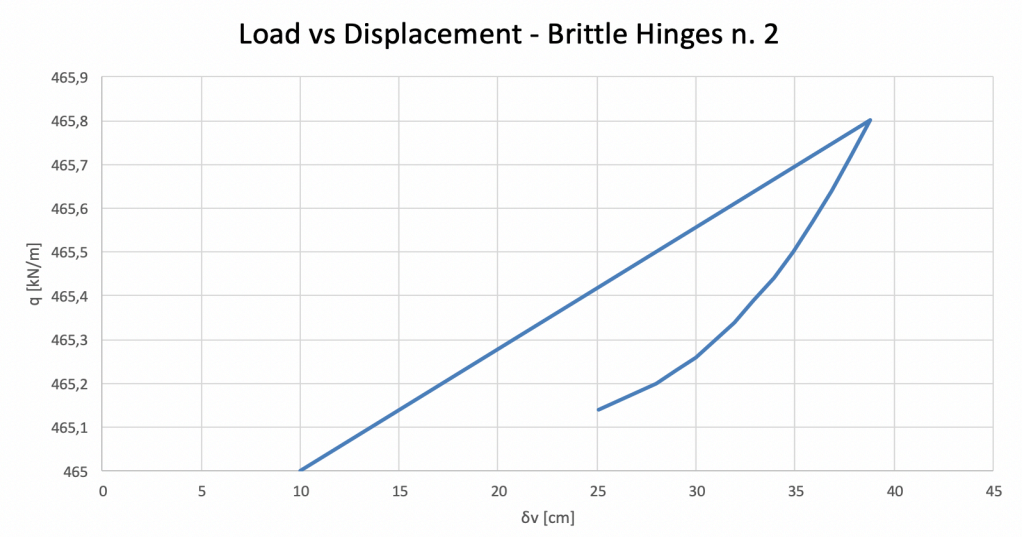

Chart 16 – Clear phenomenon of the snap-back in the second group of the brittle hinges in the Mosca Bridge

Equally as done for arches with degree of lowering equal to 1/5, to 1/6 and to 1/7, note the values of the live load q, which is remembered to have been calculated in crack opening control (w), in a subsequent phase the overall structure of the arch was calculated for each iteration step of the initialization phase 1 and 2 vertical displacement, measured in the arch crown with the finite elements. This model of the calculation was assigned the uniformly distributed load q, derived from the two previous phases:

3. For the first phase of initialization the moment of inertia of the section has been reduced in correspondence with the crack (section n. 2 and n. 16) to take into account, at each step, the progress of the real crack tip and therefore of the portion section no longer reagent;
4. For the second initialization phase a hinge was introduced in the completely cracked sections from the previous phase (section n. 2 and n. 16) and we proceeded as described in the previous point to take into account the progressive advancement of the crack (in the section n. 8, n. 9 and n. 13).

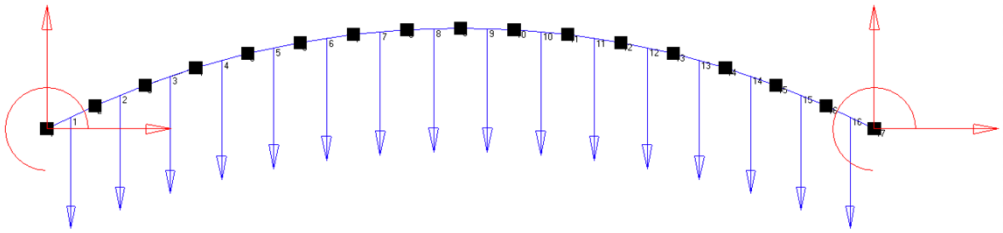

Figure 43 – FEM calculation scheme of Mosca Bridge.

For each loading phase, the vertical displacement in the arch crown was measured. The following table shows the results obtained:

q [kN/m]	δ [cm]
0.00	0.01878232
364.59	0.1493562
364.03	0.1498205
363.50	0.1504727
363.03	0.1513845
362.61	0.1526517
362.23	0.1544193
361.91	0.1569171

q [kN/m]	δ [cm]
361.63	0.1605234
361.39	0.165888
361.19	0.1741812
361.02	0.187634
360.88	0.21078
360.77	0.2534892
360.68	0.33855189
360.62	0.35178052
465.80	0.3568921
465.72	0.3915207
465.64	0.4324286
465.57	0.4806732
465.50	0.5372213
465.44	0.6029462
465.39	0.6783479
465.34	0.7633233
465.30	0.8570634
465.26	0.9582355
465.23	1.066252
465.20	1.170155
465.18	1.330334
465.16	1.563011
465.14	2.112796

Therefore, plotting the results obtained we find:

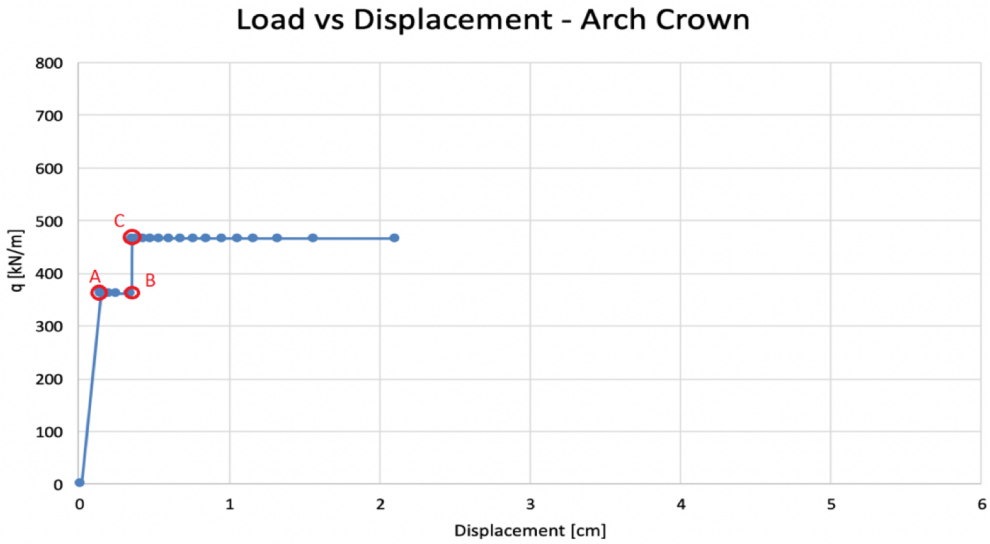

Chart 17 - Trend of the displacement of the arch crown due to the variation of the live load q in Mosca Bridge.

In Chart 17, points A, B and C are highlighted. These points represent:

A: starting point of the cracking process in sections 2 and 16;

B: points for reaching the maximum extension of the crack in sections 2 and 16 and formation of brittle hinges;

C: starting point of the cracking process in sections 8, 9 and 10 due to the new loading process due to the change in the static scheme of the arch.

In this case, looking at the Chart 17, the snap-through phenomenon is clearly visible. However, looking at a focus of the Chart 18 the "jump" linked to the instability is clearer:

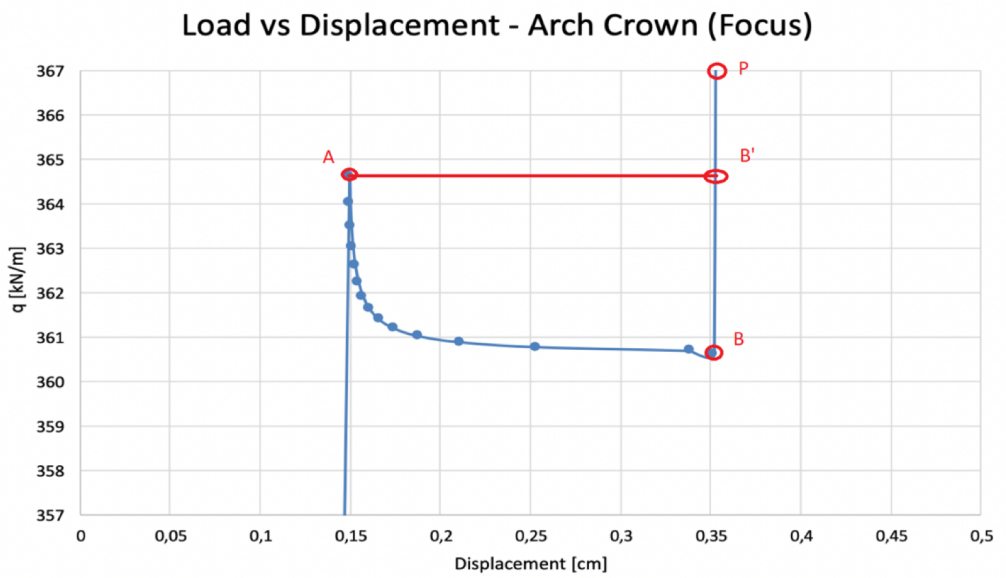

Chart 18 – Focus of the Chart 17 where the phenomenon of the snap-through is clearly visible.

In the same way as the case seen in the previous chapter, we notice the phenomenon of the snap-through. In fact, having arrived at the stationary point A, if we continue to increase the load q, it jumps discontinuously on the stable branch B'-P (to see Chart 18), which at a similar load shows a significantly greater lowering. From an energetic point of view, the energy returned by the system in jump A-B 'is equal to the area subtended by the line AB', for the length of the arch. This energy will be transformed into the kinetic vibrational energy of the system around the condition represented by the point B'.

In conclusion, Figure 44 schematically shows the position of the n. 5 brittle hinges obtained.

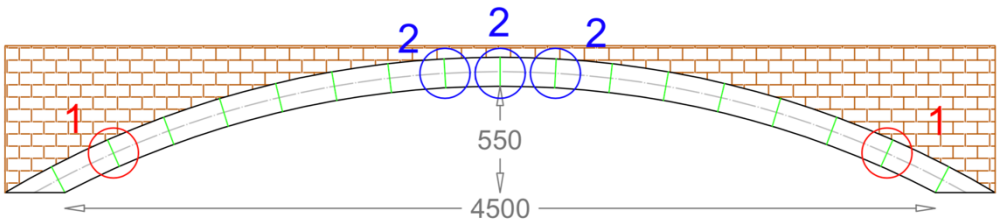

Figure 44 – Position of the brittle hinges in Mosca Bridge.

Conclusion

In this thesis work, the model of the cohesive crack was applied to bridges with masonry arches, using a program written in Matlab. The purpose of this application was to determine the maximum live load that the arches under examination can withstand before reaching the formation, by cracking or by reaching the maximum compressive strength, of n. 4 brittle hinges. The analyzed arches have a degree of lowering equal to 1/3, 1/4, 1/5, 1/6, 1/7 and about 1/8 (Moscow Bridge). From the application of the program written in Matlab it was found that for a degree of lowering greater than and equal to 1/4 the maximum live load borne does not cause cracking but the crushing in the sections where the formation of brittle hinges is found. Below the aforementioned degree of lowering the formation of the n. 4 hinges occur due to the birth and development of the cracking process. Following the cracking process by means of the cohesive model theory, i.e. by varying the load in control of the crack opening, it was found, in the sections in which crack propagation occurred and for all arches with lower and equal lowering degree 1/5, a behavior of the snap-back type material. This behavior is entirely plausible for materials of a relatively fragile type such as masonry, but readable only if the analysis is carried out in control of the gap opening and not in

displacement control or in load control. While, analyzing the same arches from a global point of view, a structural snap-through behavior was found.

In conclusion it was shown how the cohesive model allows us to grasp the real behavior of the material.

Moreover, from the analysis it is also found that the first pair of crack is formed near the section to the kidneys while the position of the second pair is linked to the degree of lowering of the arch. In fact, it has been noted that, as the degree of lowering decreases, the position of the second pair moves more and more towards the arch crown, that is, we are getting closer and closer to a beam behavior.

References

Accornero, F., Lacidogna, G., Carpinteri, A., (2018) "*Medieval Arch Bridges in the Lanzo Valleys, Italy: Case Studies on Incremental Structural Analysis and Fracturing Benefit*", ASCE, J. Bridge Eng., 23(7).

Block, P., Dejong, M., Ochsendorf, J., (2006) "*As Hangs the Flexible Line: Equilibrium of Masonry Arches*", Nexus Network Journal, Vol. 8: 9-17.

Brencich, A., Morbiducci, R., (2007) "*Masonry Arches: Historical Rules and Moderm Mechanics*", International Journal of Architectural Heritage, 1:2, 165-189.

Chiorino, M.A., Icardi, A.G., Rolando, S.V., Testa, M.F., "*Mechanism and finite element failure analysis of Mosca's bridge over the Dora in Turin*", Department of Structural and Geotechnical Engineering, Politecnico di Torino, Italy.

Accornero, F., Lacidogna, G., Carpinteri, A., (2016) "Evolutionary fracture analysis of masonry arches: Effects of shallowness ratio and size scale", C.R. Macanique 344 (2016) 623-630.

Gilibert, M., "*Limit analysis applied to masonry arch bridges: state-of-the-art and recent developments*", University of Sheffield, Department of Civil & Structural Engineering, Sheffield, UK.

Carpinteri, A., ASCE, F., Lacidogna, G., Accornero, F., (2015) "*Evolution of the Fracturing Process in Masonry Arches*", J. Struct. Eng., 141(5).

Jurina, L., (2002) "*Verifiche statiche ed interventi di consolidamento nei ponti in muratura*", Seminario CIAS, Bolzano 2002.

Jurina, L., (2004) "Ponti in muratura: *Verifiche statiche ed interventi di consolidamento nei ponti in muratura*", Seminario CIAS, Bolzano 2004.

Jurina, L., (2005) "Ponti in muratura: *Difetti e patologie*", Seminario CIAS, Bolzano 2005.

Roca, P., Cervera, M., Gariup, L.P., (2010) "*Strucutarl Analysis of Masonry Histical Constructions. Classical and Advanced Approaches*", Arc. Comput Methods Eng. 17: 299-325.

De Nicolo, B., Meloni, D., "*Modellazione di volte e archi in muratura",* Dipartimento di Ingegneria strutturale, Università di Cagliari, Modellazione FEM di archi e volte in muratura, 122-147.

Oliviera, D., (2005) "*Strengthening of stone masonry arch bridges: Three leaf masonry wall-state of the art*", Universidade do Minho, Escola de Engenharia, Guimaraes, Portugal.

Carpinteri, A., Corrado, M., Mancini, G., Paggi, M., (2009) "*Il modello della fessura coesiva in trazione e compressione per la valutazione della duttilità degli elementi strutturali in calcestruzzo armato*", Frattura ed Integrità Strutturale 7: 17-28.

Minotti, M., Salvini, P., Mannucci, G., (2009) "*Modello coesivo per l'avanzamento di fratture mediante rilascio nodale di strutture discretizzate con elementi finiti*", Frattura ed Integrità Strutturale 11: 36-48.

Carpinteri, A., "*Meccanica della frattura*", Torino, Pitagora Editrice Bologna, 1992.

Barpi F., "*Modelli numerici per lo studio dei fenomeni fessurativi nelle dighe*", Doctoral thesis, Departiment of Structural, Geotechnical and Bulding Engineering, Politecnico di Torino, Tutor Prof. Valente S., Coordinator Prof. Carpinteri A.,1996.

Appendix – MATLAB code

```
function [risultati]=biutarc
    %Parameters: constant for all beams
E = 300000; b=100;  h=150;    A = b*h;    I = (b*h^3)/12;     fc= -500;   ft=15;
%  { kg*cm^2} {cm}    {cm}      {cm^2}          {cm^4}             {kg*cm^2}  {kg*cm^-2}
  puv=25*10^-4;      H=1110;    gf=14;
  %  {kg*cm^-3}       {cm}     {kg/cm}
%vettore aus
 aus=[-0.00014488;  -0.00013582; -0.00012786;   -0.00011999;   -0.00011219;
-0.00010442;    -0.00009666;    -0.00008891;    -0.00008116;    -0.00007341;
-0.00006566;    -0.00005791;    -0.00005015;    -0.00004239;    -0.00003461;
-0.0000268;     -0.00001891;    -0.00001068;    -0.00013582;    -0.00012875;
-0.00012102;    -0.00011357;    -0.00010619;    -0.00009883;    -0.00009148;
-0.00008414;    -0.00007681;    -0.00006948;    -0.00006215;    -0.00005481;
-0.00004747;    -0.00004013;    -0.00003276;    -0.00002538;    -0.00001791;
-0.00001012;    -0.00012786;    -0.00012102;    -0.00011444;    -0.00010719;
-0.00010019;    -0.00009323;    -0.0000863;     -0.00007938;    -0.00007246;
-0.00006555;    -0.00005863;    -0.00005172;    -0.00004479;    -0.00003786;
-0.00003092;    -0.00002395;    -0.00001691;    -0.00000956;    -0.00011999;
-0.00011357;    -0.00010719;    -0.00010105;    -0.00009423;    -0.00008766;
-0.00008113;    -0.00007462;    -0.00006812;    -0.00006162;    -0.00005512;
-0.00004862;    -0.00004211;    -0.0000356;     -0.00002908;    -0.00002253;
-0.0000159;     -0.00000899;    -0.00011219;    -0.00010619;    -0.00010019;
-0.00009423;    -0.00008851;    -0.00008213;    -0.00007598;    -0.00006987;
-0.00006378;    -0.00005769;    -0.00005161;    -0.00004552;    -0.00003944;
-0.00003334;    -0.00002723;    -0.00002111;    -0.0000149;     -0.00000843;
-0.00010442;    -0.00009883;    -0.00009323;    -0.00008766;    -0.00008213;
-0.00007683;    -0.00007086;    -0.00006513;    -0.00005944;    -0.00005377;
-0.0000481;     -0.00004243;    -0.00003676;    -0.00003108;    -0.00002539;
-0.00001968;    -0.0000139;     -0.00000787;    -0.00009666;    -0.00009148;
-0.0000863;     -0.00008113;    -0.00007598;    -0.00007086;    -0.00006598;
-0.00006044;    -0.00005512;    -0.00004985;    -0.00004459;    -0.00003934;
-0.00003408;    -0.00002882;    -0.00002355;    -0.00001826;    -0.0000129;
-0.00000731;    -0.00008891;    -0.00008414;    -0.00007938;    -0.00007462;
-0.00006987;    -0.00006513;    -0.00006044;    -0.00005598;    -0.00005084;
-0.00004595;    -0.00004109;    -0.00003625;    -0.0000314;     -0.00002656;
-0.00002171;    -0.00001683;    -0.0000119;     -0.00000675;    -0.00008116;
-0.00007681;    -0.00007246;    -0.00006812;    -0.00006378;    -0.00005944;
-0.00005512;    -0.00005084;    -0.0000468;     -0.00004208;    -0.0000376;
-0.00003316;    -0.00002873;    -0.0000243;     -0.00001986;    -0.00001541;
-0.0000109;     -0.00000618;    -0.00007341;    -0.00006948;    -0.00006555;
-0.00006162;    -0.00005769;    -0.00005377;    -0.00004985;    -0.00004595;
-0.00004208;    -0.00003846;    -0.00003416;    -0.00003009;    -0.00002607;
-0.00002205;    -0.00001802;    -0.00001399;    -0.0000099;     -0.00000562;
-0.00006566;    -0.00006215;    -0.00005863;    -0.00005512;    -0.00005161;
-0.0000481;     -0.00004459;    -0.00004109;    -0.0000376;     -0.00003416;
-0.00003095;    -0.00002706;    -0.00002341;    -0.0000198;     -0.00001619;
-0.00001257;    -0.0000089;     -0.00000506;    -0.00005791;    -0.00005481;
-0.00005172;    -0.00004862;    -0.00004552;    -0.00004243;    -0.00003934;
-0.00003625;    -0.00003316;    -0.00003009;    -0.00002706;    -0.00002427;
-0.0000208;     -0.00001756;    -0.00001435;    -0.00001115;    -0.0000079;
-0.0000045;     -0.00005015;    -0.00004747;    -0.00004479;    -0.00004211;
-0.00003944;    -0.00003676;    -0.00003408;    -0.0000314;     -0.00002873;
-0.00002607;    -0.00002341;    -0.0000208;     -0.00001842;    -0.00001536;
-0.00001253;    -0.00000973;    -0.0000069;     -0.00000393;    -0.00004239;
-0.00004013;    -0.00003786;    -0.0000356;     -0.00003334;    -0.00003108;
```

```
-0.00002882;     -0.00002656;    -0.0000243;     -0.00002205;    -0.0000198;
-0.00001756;     -0.00001536;    -0.0000134;     -0.00001075;    -0.00000833;
-0.0000059;      -0.00000337;    -0.00003461;    -0.00003276;    -0.00003092;
-0.00002908;     -0.00002723;    -0.00002539;    -0.00002355;     -0.00002171;
-0.00001986;     -0.00001802;    -0.00001619;    -0.00001435;    -0.00001253;
-0.00001075;     -0.0000092;     -0.00000696;    -0.00000492;    -0.00000281;
-0.0000268;      -0.00002538;    -0.00002395;    -0.00002253;    -0.00002111;
-0.00001968;     -0.00001826;    -0.00001683;    -0.00001541;    -0.00001399;
-0.00001257;     -0.00001115;    -0.00000973;    -0.00000833;    -0.00000696;
-0.00000581;     -0.00000396;    -0.00000226;    -0.00001891;    -0.00001791;
-0.00001691;     -0.0000159;     -0.0000149;     -0.0000139;     -0.0000129;
-0.0000119;      -0.0000109;     -0.0000099;     -0.0000089;     -0.0000079;
-0.0000069;      -0.0000059;     -0.00000492;    -0.00000396;    -0.00000322;
-0.00000173;     -0.00001068;    -0.00001012;    -0.00000956;    -0.00000899;
-0.00000843;     -0.00000787;    -0.00000731;    -0.00000675;    -0.00000618;
-0.00000562;     -0.00000506;    -0.0000045;     -0.00000393;    -0.00000337;
-0.00000281;     -0.00000226;    -0.00000173;    -0.00000138]

 %vettore df
 df=[-0.00029272; -0.00027688; -0.00026104; -0.00024519; -0.00022934; -0.00021347;
-0.00019761; -0.00018173; -0.00016585; -0.00014996; -0.00013406; -0.00011816; -
0.00010225; -0.00008633; -0.0000704; -0.00005442; -0.0000383; -0.00002155];

%ponte Mosca H=760 cm
%x=[0 263.2433 533.6215 810.1636 1091.8765 1377.7485 1666.7529 1957.8519 2250
2542.1481 2833.2471 3122.2515 3408.1235 3689.8364 3966.3785 4236.7567 4500];
%y=[0 127.0047 238.013 332.6265 410.5052 471.3694 515.0007 541.2423  550 541.2423
515.0007 471.3694 410.5052 332.6265 238.013 127.0047 0];

%f/l=1/3 l=4500 cm e f=1500 cm H=1710 cm
%x=[0 148.07 353.88 601.46 885.32 1199.39 1536.42 1889.82 2250 2610.18 2963.58
3300.61 3614.68 3898.54 4146.12 4351.93 4500];
%y=[0 296.71 594.21 857.98 1082.17 1260.46 1393.21 1473.24 1500 1473.24 1393.21
1260.46 1082.17 857.98 594.21 296.71 0];

%f/l=1/4 l=4500 cm e f=1125 cm H=1335 cm
%x=[0 210.26 447.90 709.72 992.21 1291.58 1603.83 1924.73 2250 2575.27 2896.17
3208.42 3507.79 3790.28 4052.10 4289.74 4500];
%y=[0 248.90 471.80 665.73 828.08 956.66 1049.77 1106.13 1125 1106.13 1049.77
956.66 828.08 665.73 471.80 248.90 0];

%f/l=1/5 l=4500 cm e f=900 cm H=1110 cm
%x=[0 234.55 487.35 756.10 1038.34 1331.54 1632.98 1940.11 2250 2559.89 2867.02
3168.45 3461.66 3743.90 4012.65 4265.45 4500];
%y=[0 201.52 382.85 537.87 666.66 768.05 841.12 885.25 900 885.25 841.12 768.05
666.66 437.87 382.85 201.52 0];

%f/l=1/6 l=4500 cm e f=750 cm H=960 cm
%x= [0 248.29 509.61 782.13 1064.15 1353.83 1649.32 1948.68 2250 2551.32 2850.68
3146.17 3435.85 3717.87 3990.39 4251.71 4500];
%y= [0 171.06 321.68 450.77 557.56 641.34 701.58 737.87 750 737.87 701.58 641.34
557.56 450.77 321.68 171.06 0];

%f/l=1/7 l=4500 cm e f=642.80 cm H=853 cm
```

```
%x= [0 256.84 523.31 798.14 1079.98 1367.72 1659.3 1953.92 2250 2546.08 2840.70
3132.28 3420.02 3701.86 3976.69 4243.16 4500];
%y= [0 147.66 277.10 387.71 478.95 550.42 601.64 632.50 642.8 632.5 601.64 550.42
478.95 387.71 277.10 147.66 0];

%Fessurazione modello coesivo
%Initializations
stiffness=zeros(16,1); q=0.0;
[M,N,sez_cal]=fem(x,y,q,E,I,A,b,puv,H,stiffness);
O=sez_cal;
%definizione nodi nella sezione
deltah=h/17;
for i=1:18
    if i==1
        z(i)=0;
    else
        z(i)=z(i-1)+i*deltah
    end
    z=z'
end
[csw,wc]=legge_costitutiva(ft,gf,N,sez_cal,A);
[P,beta] = calcolo_carico(x,y,H,b,puv,sez_cal,q);
ntip=1;
ntipa=1;
nnod=18;
q_coesivo=0;
k=1;
G=0;
u=0;
e=0;
o=0;
t=0;
    while ntipa<=15
        [N,M]=Cal_N(x,y,q_coesivo,E,I,A,b,puv,H,stiffness,sez_cal);
        sigmat=ft+(N*(-1))/A;
        [coe,ab]=letcoe(aus,nnod,ntipa,ntip,csw,z,wc);
        [p,w,abb]=soluz(coe,P,ntipa,ntip,nnod,df);
        abft=ab*sigmat;
        if ntip==1
            deltaf=(abft/p);
        else
            if ntip~=18
                deltaf=(abft-pold)/(p-pold);
            else
                deltaf=deltaf
            end
        end
        P=P+deltaf;
        pold=p
        G(k)=P
        u(k)=abb*cos(beta)
        e(k)=N
        if ntip~=18
            ntip=ntip+1;
        else
```

```
        ntip==18
    end
    if w>=wc
        ntipa=ntipa+1;
    else
        ntipa=ntipa;
    end
    t(k)=ntipa
    k=k+1
    F=P
    [q_coesivo]=load_variable(F,x,y,H,b,puv,sez_cal);
    o(k)=q_coesivo;
end
[q_coesivo]=load_variable(F,x,y,H,b,puv,sez_cal);
plot(u,G);
crush=0;
 while crush==0
    [M,N]=fem(x,y,q,E,I,A,b,puv,H,stiffness);
    crush=crushing_collapse(M, N, h, abs(fc), I, A);
    if  crush==1
        q_classic=q;
    end
    %Load increase
    q=q+0.01;
end
disp(q_classic);
disp(q_coesivo);
disp(ntipa);
disp(ntip);
```

```
function [N,M]=Cal_N(x,y,q_coesivo,E,I,A,b,puv,H,stiffness,sez_cal)
%Initializations
rigidezza_definitiva=zeros(51,51);  q_definitiva=zeros(51,1);   indice=1;
%Ciclo spostamenti
for k=1:16

    L=sqrt((x(k+1)-x(k))^2 + (y(k+1)-y(k))^2);
    alpha=atan((y(k+1)-y(k))/(x(k+1)-x(k)));
    assemblaggio=zeros(51,6);


    kloc =    (E*I).*[ 4/L,     -6/L^2,     0,      2/L,      6/L^2,      0;
                      -6/L^2,    12/L^3,    0,     -6/L^2,   -12/L^3,     0;
                        0,          0,     A/(I*L),  0,          0,      -A/(I*L);
                        2/L,     -6/L^2,     0,     4/L,       6/L^2,      0;
                        6/L^2,   -12/L^3,    0,     6/L^2,     12/L^3,     0;
                        0,          0,   -A/(I*L),    0,          0,       A/(I*L)];

  rot = [     1,      0,          0,               0,      0,              0;
                0,  cos(alpha),     sin(alpha),     0,      0,              0;
                0,  -sin(alpha),    cos(alpha),     0,      0,              0;
                0,      0,          0,              1,      0,              0;
                0,      0,          0,              0,  cos(alpha),     sin(alpha);
                0,      0,          0,              0, -sin(alpha),    cos(alpha)];

    if stiffness(k)~=0
        %Moltiplico *EI non refresha
        kloc(1,1)=E*I*(3*E*I+4*L*stiffness(k))/(L*(E*I+L*stiffness(k)));
        kloc(1,4)=E*I*(3*E*I+2*L*stiffness(k))/(L*(E*I+L*stiffness(k)));
        kloc(4,1)=E*I*(3*E*I+2*L*stiffness(k))/(L*(E*I+L*stiffness(k)));
        kloc(4,4)=E*I*(3*E*I+4*L*stiffness(k))/(L*(E*I+L*stiffness(k)));
    end

    kglob = rot'*kloc*rot;

    %Carico equivalente nodale
    p_proprio=(puv*b*((H-y(k))+(H-y(k+1))))*(1/2);

        Q=[-
((q_coesivo+p_proprio)*cos(alpha)*L^2)/12,((q_coesivo+p_proprio)*cos(alpha)*L/2),-
((q_coesivo+p_proprio)*sin(alpha)*L/2),
((q_coesivo+p_proprio)*cos(alpha)*L^2)/12,((q_coesivo+p_proprio)*cos(alpha)*L/2),-
((q_coesivo+p_proprio)*sin(alpha)*L/2)]';
    %Matrice assemblaggio
    switch k
       case 1
       assemblaggio(1:3,4:6)=eye(3);
       assemblaggio(46:48,1:3)=eye(3);
       case 16
       assemblaggio(43:45,1:3)=eye(3);
       assemblaggio(49:51,4:6)=eye(3);
       otherwise
       assemblaggio(indice:indice+5,1:6)=eye(6);
       indice=indice+3;
```

```
    end

    %Assemblaggio carico
    q_definitiva=q_definitiva+assemblaggio*Q;
    %Assemblaggio rigidezza
    rigidezza_definitiva=rigidezza_definitiva+assemblaggio*kglob*assemblaggio';
end

spostamenti_ll=rigidezza_definitiva(1:45,1:45)\q_definitiva(1:45);

%PROVA
%reazioni=rigidezza_definitiva(46:51,1:45)*spostamenti_ll-q_definitiva(46:51);
%[reazione1,reazione2]=calcolo_reazioni(reazioni,x,y);
%FINE PROVA

%Ciclo calcolo MTN per ciascuna trave
MTN=zeros(102,1); indice=1; spostamenti_LL=zeros(51,1);
spostamenti_LL(4:48)=spostamenti_ll(1:45); index=1;
for k=1:16

    L=sqrt((x(k+1)-x(k))^2 + (y(k+1)-y(k))^2);
    alpha=atan((y(k+1)-y(k))/(x(k+1)-x(k)));

    kloc =     (E*I).*[ 4/L,   -6/L^2,   0,       2/L,       6/L^2,      0;
                       -6/L^2,   12/L^3,  0,      -6/L^2,   -12/L^3 ,     0;
                         0,        0,   A/(I*L),     0,         0,      -A/(I*L);
                         2/L,    -6/L^2,   0,       4/L,      6/L^2,      0;
                         6/L^2,  -12/L^3,  0,      6/L^2,      12/L^3,    0;
                         0,         0,   -A/(I*L),   0,          0,     A/(I*L)];

    rot = [     1,      0,          0,              0,      0,              0;
                0,  cos(alpha),     sin(alpha),     0,      0,              0;
                0,  -sin(alpha),    cos(alpha),     0,      0,              0;
                0,      0,          0,              1,      0,              0;
                0,      0,          0,              0,   cos(alpha),   sin(alpha);
                0,      0,          0,              0   -sin(alpha),   cos(alpha)];

    if stiffness(k)~=0
        %Moltiplico *EI non refresha
        kloc(1,1)=E*I*(3*E*I+4*L*stiffness(k))/(L*(E*I+L*stiffness(k)));
        kloc(1,4)=E*I*(3*E*I+2*L*stiffness(k))/(L*(E*I+L*stiffness(k)));
        kloc(4,1)=E*I*(3*E*I+2*L*stiffness(k))/(L*(E*I+L*stiffness(k)));
        kloc(4,4)=E*I*(3*E*I+4*L*stiffness(k))/(L*(E*I+L*stiffness(k)));
    end

    spostamenti_locali=rot*spostamenti_LL(indice:indice+5,1);
    Q=[-
((q_coesivo+p_proprio)*cos(alpha)*L^2)/12,((q_coesivo+p_proprio)*cos(alpha)*L/2),-
((q_coesivo+p_proprio)*sin(alpha)*L/2),
((q_coesivo+p_proprio)*cos(alpha)*L^2)/12,((q_coesivo+p_proprio)*cos(alpha)*L/2),-
((q_coesivo+p_proprio)*sin(alpha)*L/2)]';


    MTN_singola=kloc*spostamenti_locali-rot*Q;
```

```
    MTN(index:index+5,1)=MTN_singola(1:6);
    indice=indice+3;
    index=index+6;
end
%Arco simmetrico, se vuoi migliora. A questo punto in MTN hai gli sforzi
%agli estremi di ogni beam, visti sia da destra sia da sinistra:
%lenght(MTN)=2*num.beam
indice=1;
M=zeros(17,1); N=zeros(17,1); T=zeros(17,1);
for k=1:6:54
    M(indice)=-MTN(k);
    T(indice)=MTN(k+1);
    N(indice)=-abs(MTN(k+2));
    indice=indice+1;
end
N=N(sez_cal);
M=M(sez_cal);
```

```
function [P,beta] = calcolo_carico(x,y,H,b,puv,sez_cal,q)
%valutazioene del fattore di carico

 if sez_cal==1
    ma=(x(sez_cal+1)-x(sez_cal))^2*((H-y(sez_cal+1)))*0.5
    mb=(1/6)*(x(sez_cal+1)-x(sez_cal))^2*((y(sez_cal+1)-y(sez_cal)))
    R=((H-y(sez_cal))+(H-y(sez_cal+1)))*(x(sez_cal+1)-x(sez_cal))*0.5
    c=(ma+mb)/R
    alpha=atan((y(sez_cal+1)-y(sez_cal))/(x(sez_cal+1)-x(sez_cal)))
    d=c*tan(alpha)
    e=0.5*c*b*((H-y(sez_cal)-d)+(H-y(sez_cal)))
    l=c
    delta=alpha
else
    ma=(1/3)*((y(sez_cal)-y(sez_cal-1))*(x(sez_cal)-x(sez_cal-1))^2)
    mb=0.5*(H-y(sez_cal))*((x(sez_cal)-x(sez_cal-1))^2)
    R1=0.5*((H-y(sez_cal-1))+(H-y(sez_cal))*(x(sez_cal)-x(sez_cal-1)))
    c1=(ma+mb)/R1
    alpha=atan((y(sez_cal)-y(sez_cal-1))/(x(sez_cal)-x(sez_cal-1)))
    d=c1*tan(alpha)
    e1=0.5*b*c1*((H-y(sez_cal))+(H-y(sez_cal-1)-d))
    md=(1/6)*(y(sez_cal+1)-y(sez_cal))*((x(sez_cal+1)-x(sez_cal))^2)
    mc=0.5*(H-y(sez_cal+1))*(x(sez_cal+1)-x(sez_cal))
    R2=0.5*((H-y(sez_cal))+(H-y(sez_cal+1)))*(x(sez_cal+1)-x(sez_cal))
    c2=(md+mc)/R2
    gamma=atan((y(sez_cal+1)-y(sez_cal))/(x(sez_cal+1)-x(sez_cal)))
    g=((x(sez_cal+1)-x(sez_cal))-c2)*tan(gamma)
    e2=0.5*c2*b*((H-y(sez_cal)-g)+(H-y(sez_cal+1)))
    e=e1+e2
    l=c1+c2
    delta=(alpha+gamma)/2
 end
P=(e*puv+l*q)*cos(delta)
beta=delta
```

```
function [crush]=crushing_collapse(M, N, h, fc, I, A)
%fc viene passata in modulo
crush=0;

for i=1:17
    if abs(M(i))*h/(2*I)+abs(N(i))/A>fc
        crush=1;
    end
end
```

```
function [M,N,sez_cal]=fem(x,y,q,E,I,A,b,puv,H,stiffness)
%Initializations
rigidezza_definitiva=zeros(51,51);  q_definitiva=zeros(51,1);   indice=1;
%Ciclo spostamenti
for k=1:16

    L=sqrt((x(k+1)-x(k))^2 + (y(k+1)-y(k))^2);
    alpha=atan((y(k+1)-y(k))/(x(k+1)-x(k)));
    assemblaggio=zeros(51,6);


    kloc =     (E*I).*[ 4/L     ,   -6/L^2      ,   0           ,   2/L     ,
6/L^2   ,   0;
                       -6/L^2    ,   12/L^3      ,   0           ,   -6/L^2  ,   -
12/L^3 ,   0;
                         0       ,   0           ,   A/(I*L)     ,   0       ,   0
,   -A/(I*L);
                         2/L     ,   -6/L^2      ,   0           ,   4/L     ,
6/L^2   ,   0;
                         6/L^2   ,   -12/L^3     ,   0           ,   6/L^2   ,
12/L^3  ,   0;
                         0       ,   0           ,   -A/(I*L)    ,   0       ,   0
,   A/(I*L)];

    rot = [     1,      0,          0,              0,      0,              0;
                0,  cos(alpha),     sin(alpha),     0,      0,              0;
                0,  -sin(alpha),    cos(alpha),     0,      0,              0;
                0,      0,          0,              1,      0,              0;
                0,      0,          0,              0,  cos(alpha),     sin(alpha);
                0,      0,          0,              0, -sin(alpha),    cos(alpha)];

    if stiffness(k)~=0
        %Moltiplico *EI non refresha
        kloc(1,1)=E*I*(3*E*I+4*L*stiffness(k))/(L*(E*I+L*stiffness(k)));
        kloc(1,4)=E*I*(3*E*I+2*L*stiffness(k))/(L*(E*I+L*stiffness(k)));
        kloc(4,1)=E*I*(3*E*I+2*L*stiffness(k))/(L*(E*I+L*stiffness(k)));
        kloc(4,4)=E*I*(3*E*I+4*L*stiffness(k))/(L*(E*I+L*stiffness(k)));
    end

    kglob = rot'*kloc*rot;

    %Carico equivalente nodale
    p_proprio=(puv*b*((H-y(k))+(H-y(k+1))))*(1/2);

        Q=[-((q+p_proprio)*cos(alpha)*L^2)/12,((q+p_proprio)*cos(alpha)*L/2),-
((q+p_proprio)*sin(alpha)*L/2),
((q+p_proprio)*cos(alpha)*L^2)/12,((q+p_proprio)*cos(alpha)*L/2),-
((q+p_proprio)*sin(alpha)*L/2)]';
    %Matrice assemblaggio
    switch k
       case 1
       assemblaggio(1:3,4:6)=eye(3);
       assemblaggio(46:48,1:3)=eye(3);
       case 16
```

```
        assemblaggio(43:45,1:3)=eye(3);
        assemblaggio(49:51,4:6)=eye(3);
        otherwise
        assemblaggio(indice:indice+5,1:6)=eye(6);
        indice=indice+3;
    end

    %Assemblaggio carico
    q_definitiva=q_definitiva+assemblaggio*Q;
    %Assemblaggio rigidezza
    rigidezza_definitiva=rigidezza_definitiva+assemblaggio*kglob*assemblaggio';
end

spostamenti_ll=rigidezza_definitiva(1:45,1:45)\q_definitiva(1:45);

%PROVA
%reazioni=rigidezza_definitiva(46:51,1:45)*spostamenti_ll-q_definitiva(46:51);
%[reazione1,reazione2]=calcolo_reazioni(reazioni,x,y);
%FINE PROVA

%Ciclo calcolo MTN per ciascuna trave
MTN=zeros(102,1); indice=1; spostamenti_LL=zeros(51,1);
spostamenti_LL(4:48)=spostamenti_ll(1:45); index=1;
for k=1:16

    L=sqrt((x(k+1)-x(k))^2 + (y(k+1)-y(k))^2);
    alpha=atan((y(k+1)-y(k))/(x(k+1)-x(k)));

    kloc =      (E*I).*[ 4/L     ,    -6/L^2      ,    0           ,    2/L     ,
6/L^2    ,    0;
                        -6/L^2    ,    12/L^3      ,    0           ,    -6/L^2  ,    -
12/L^3 ,    0;
                          0       ,    0           ,    A/(I*L)     ,    0       ,    0
,    -A/(I*L);
                          2/L     ,    -6/L^2      ,    0           ,    4/L     ,
6/L^2    ,    0;
                          6/L^2   ,    -12/L^3     ,    0           ,    6/L^2   ,
12/L^3   ,    0;
                          0       ,    0           ,    -A/(I*L)    ,    0       ,    0
,    A/(I*L)];

    rot = [     1,      0,          0,              0,      0,              0;
                0,  cos(alpha),     sin(alpha),     0,      0,              0;
                0,  -sin(alpha),    cos(alpha),     0,      0,              0;
                0,      0,          0,              1,      0,              0;
                0,      0,          0,              0,      cos(alpha),
sin(alpha);
                0,      0,          0,              0,      -sin(alpha),
cos(alpha)];

    if stiffness(k)~=0
        %Moltiplico *EI non refresha
        kloc(1,1)=E*I*(3*E*I+4*L*stiffness(k))/(L*(E*I+L*stiffness(k)));
        kloc(1,4)=E*I*(3*E*I+2*L*stiffness(k))/(L*(E*I+L*stiffness(k)));
```

```
        kloc(4,1)=E*I*(3*E*I+2*L*stiffness(k))/(L*(E*I+L*stiffness(k)));
        kloc(4,4)=E*I*(3*E*I+4*L*stiffness(k))/(L*(E*I+L*stiffness(k)));
    end

    spostamenti_locali=rot*spostamenti_LL(indice:indice+5,1);
    Q=[-((q+p_proprio)*cos(alpha)*L^2)/12,((q+p_proprio)*cos(alpha)*L/2),-
((q+p_proprio)*sin(alpha)*L/2),
((q+p_proprio)*cos(alpha)*L^2)/12,((q+p_proprio)*cos(alpha)*L/2),-
((q+p_proprio)*sin(alpha)*L/2)]';


    MTN_singola=kloc*spostamenti_locali-rot*Q;
    MTN(index:index+5,1)=MTN_singola(1:6);
    indice=indice+3;
    index=index+6;
end
%Arco simmetrico. A questo punto in MTN hai gli sforzi
%agli estremi di ogni beam, visti sia da destra sia da sinistra:
%lenght(MTN)=2*num.beam
indice=1;
M=zeros(17,1); N=zeros(17,1); T=zeros(17,1);
for k=1:6:54
    M(indice)=-MTN(k);
    T(indice)=MTN(k+1);
    N(indice)=-abs(MTN(k+2));
    indice=indice+1;
end
N(10)=N(8);
N(11)=N(7);
N(12)=N(6);
N(13)=N(5);
N(14)=N(4);
N(15)=N(3);
N(16)=N(2);
N(17)=N(1);
M(10)=M(8);
M(11)=M(7);
M(12)=M(6);
M(13)=M(5);
M(14)=M(4);
M(15)=M(3);
M(16)=M(2);
M(17)=M(1);
S=abs (M)
[Mmax,sez_cal]=max (S)
```

```
function[csw,wc]=legge_costitutiva(ft,gf,N,sez_cal,A)
%definizione legge costitutiva
cws(1,2)=ft
cws(2,2)=cws(1,2)/2
cws(3,2)=0
csw(1,1)=0
csw(2,1)=0.045
csw(3,2)=0.09
nret=2
nr=nret+1
som=0.0
csw(1,2)=1
csw(nr,1)=1
wc=0,047
csw(1,1)=0.0
csw(1,2)=ft
csw(1,3)=wc
csw(1,4)=ft
csw(nr,1)=wc
csw(nr,2)=0.0
csw(nr,3)=wc
csw(nr,4)=0.0
if nret>1
    for j=2:nret
        csw(j,1)=csw(j,1)*wc
        csw(j,2)=csw(j,2)*ft
    end
    for j=2:nret
        csw(j,4)=csw(j,2)-csw(j,1)*(csw(j+1,2)-csw(j,2))/(csw(j+1,1)-csw(j,1))
    end
    for j=2:nret
        csw(j-1,3)=csw(j-1,1)-csw(j-1,2)*(csw(j,1)-csw(j-1,1))/(csw(j,2)-csw(j-
1,2))
    end
else
    csw(nret,3)=csw(nr,3)
end
```

```
function [coe,ab]=letcoe(aus,nnod,ntipa,ntip,csw,z,wc)
%Questa funzione legge i coefficienti di influenza per ogni situazione di
%carico unitaria.
%Questa funzione modifica i coefficienti della matrice coe()in modo da
%inserire il legame costitutivo e risolve il sistema.
%Questa funzione risolve un sistema di equazioni lineare. Si ricorda che le
%incognite del problema sono in parte spostamenti e in parte forze coesive
%di richiusura. Una volta calcolate si procede al calcolo delle ulteriori
%forze coesive incognite.

%Definizione variabili
  nta=ntipa-1
  nnod=18;
  ycor=0.9;
%Lettura matrice dei coefficienti di influenza
coe=[]
   nk=0
   for k=1:nnod
       if k>=ntipa
           for i=ntipa:nnod
               coe(nk+i)=aus(i)*ycor*2
           end
           nk=nk+nnod
       else
           nk=nk+nnod
       end
   end
   nk=nnod*nnod
   for i=ntipa:nnod
       coe(nk+i)=aus(i)*ycor*2
   end
if ntip==0
    ab=(z(2)-z(1))/2
else
    ab=z(2)-z(1)
end
pu=csw(1,2)*ab
nta=ntipa-1
 %correzione vettore termini noti
ncor=ntip-ntipa
nw=nnod*nnod
if ncor~=0
    for i=1:ncor
        coe(nw+nta+i)=coe(nw+nta+i)+wc
    end
end
lk=nta*nnod+nta
for i=1:ncor
    coe(lk+i)=coe(lk+i)+(wc/pu)
    lk=lk+nnod
end
%passaggio dalla vettore coe() alla matrice a[n,n] e al vettore dei
%termini noti f(n)
f=0
a=0
```

```
nwa=nnod-nta
qk=nta
if nta==0
    qk=nta
else
    qk=nta*nnod+nta
end
for j=1:nwa
    for i=1:nwa
        a(i,j)=coe(i+qk)
    end
    qk=qk+nnod
end
for b=1:nwa
    f(b)=coe(nw+b+nta)
end
o=f'
x=pinv(a)*o
%calcolo delle aperture della fessura incognite e passaggio dal vettore x() al
vettore coe()
nta=ntipa-1
nwa=nnod-nta
nw=nnod*nnod
ncor=ntip-ntipa
for i=1:nwa
    coe(nw+i+nta)=x(i)
end
if ncor>=1
    for j=1:ncor
        coe(nw+nwa+j+nta)=wc*(1-x(j)/pu)
    end
end
coe=coe'
```

```
function [q_coesivo]=load_variable(F,x,y,H,b,puv,sez_cal)
 if sez_cal==1
    ma=(x(sez_cal+1)-x(sez_cal))^2*((H-y(sez_cal+1)))*0.5
    mb=(1/6)*(x(sez_cal+1)-x(sez_cal))^2*((y(sez_cal+1)-y(sez_cal)))
    R=((H-y(sez_cal))+(H-y(sez_cal+1)))*(x(sez_cal+1)-x(sez_cal))*0.5
    c=(ma+mb)/R
    alpha=atan((y(sez_cal+1)-y(sez_cal))/(x(sez_cal+1)-x(sez_cal)))
    d=c*tan(alpha)
    e=0.5*c*b*((H-y(sez_cal)-d)+(H-y(sez_cal)))
    l=c
    delta=alpha
else
    ma=(1/3)*((y(sez_cal)-y(sez_cal-1))*(x(sez_cal)-x(sez_cal-1))^2)
    mb=0.5*(H-y(sez_cal))*((x(sez_cal)-x(sez_cal-1))^2)
    R1=0.5*((H-y(sez_cal-1))+(H-y(sez_cal))*(x(sez_cal)-x(sez_cal-1)))
    c1=(ma+mb)/R1
    alpha=atan((y(sez_cal)-y(sez_cal-1))/(x(sez_cal)-x(sez_cal-1)))
    d=c1*tan(alpha)
    e1=0.5*b*c1*((H-y(sez_cal))+(H-y(sez_cal-1)-d))
    md=(1/6)*(y(sez_cal+1)-y(sez_cal))*((x(sez_cal+1)-x(sez_cal))^2)
    mc=0.5*(H-y(sez_cal+1))*(x(sez_cal+1)-x(sez_cal))
    R2=0.5*((H-y(sez_cal))+(H-y(sez_cal+1)))*(x(sez_cal+1)-x(sez_cal))
    c2=(md+mc)/R2
    gamma=atan((y(sez_cal+1)-y(sez_cal))/(x(sez_cal+1)-x(sez_cal)))
    g=((x(sez_cal+1)-x(sez_cal))-c2)*tan(gamma)
    e2=0.5*c2*b*((H-y(sez_cal)-g)+(H-y(sez_cal+1)))
    e=e1+e2
    l=c1+c2
    delta=(alpha+gamma)/2
 end
q_coesivo=(F+e*puv*cos(delta))/(l*cos(delta))
```

```
function [p,w,abb]=soluz(coe,P,ntipa,ntip,nnod,df)
%Questa funzione prepara la matrice dei coefficienti e il vettore termini
%noti per il calcolo delle forze di richiusura dovute alla forza esterna e
%degli spostamenti dovuti alla microfessurazione.
%correzione matrice e termini noti microfessure
nw=nnod*nnod
nta=ntipa-1
nwa=nnod-nta
ncor=ntip-ntipa
for i=1:nwa
    coe(nw+nta+i)=-coe(nw+nta+i)*P
end
%memorizzazione nuove forze e spostamenti
p=0
w=0
for i=ntipa:nnod
    p(i)=coe(nw+i)
end
if ncor==0
    for i=ntipa:ntip
        w(i)=0
    end
else
    for i=1:ncor
        w(nta+i)=coe(nw+nnod+i)
    end
end
if nta>0
    for i=1:nta
        nk=nnod*nta+i
        som=0
        for j=ntipa:nnod
            som=som+coe(nk)*p(j)
            nk=nk+nnod
        end
        w(i)=som+coe(nw+i)*P
    end
end
%Calcolo spostamento del punto di carico esterno
som=0
for i=1:nnod
    som=som+df(i)*p(i)
end
abb=som+0.000157737*P
p=p(ntip)
w=w(ntipa)
```